ARMY RESEARCH LABORATORY

Comparison of Infrared and Millimeter-Wave Imager Performance in Adverse Weather Conditions

by Brian Riely

ARL-TR-1301 December 1997

The findings in this report are not to be construed as an official Department of the Army position unless so designated by other authorized documents.

Citation of manufacturer's or trade names does not constitute an official endorsement or approval of the use thereof.

Destroy this report when it is no longer needed. Do not return it to the originator.

Army Research Laboratory
Adelphi, MD 20783-1197

ARL-TR-1301 **December 1997**

Comparison of Infrared and Millimeter-Wave Imager Performance in Adverse Weather Conditions

Brian Riely
Sensors and Electron Devices Directorate

Abstract

This report compares the performance of infrared and millimeter-wave imagers in various weather conditions (rain, fog, clouds, and, to a lesser extent, snow). It then examines how often these weather conditions occur each season at selected areas around the world. The data for the frequency of occurrence of the adverse conditions were taken from a 1992 climatology module that used inputs from 795 meteorological stations around the world.

Contents

Figures

Figures (cont'd)

Tables

Tables (cont'd)

Tables (cont'd)

List

1. Introduction

The U.S. Army Research Laboratory (ARL) is investigating passive millimeter-wave (MMW) imaging technology for Army applications, particularly reconnaissance, surveillance, and target acquisition. The primary motivation for the Army's interest in this technology is that the performance of MMW imagers under adverse weather conditions generally is not seriously degraded. In addition, it is inherently covert. In clear weather, the main advantages of passive infrared (IR) imagers over MMW imagers are (1) shorter wavelength, leading to greater image resolution, and (2) greater detection range. However, under adverse weather conditions, atmospheric attenuation can prevent the detection of an IR signal. Under these same weather conditions, an MMW signal may still be easily detected. Thus, the use of passive MMW imaging technology may have some advantages over passive IR imaging systems or may play a more general role as an adjunct sensor to be used under adverse weather conditions. This report examines the weather conditions under which passive MMW imagers outperform passive IR imagers and how often these conditions occur in geographic regions where U.S. forces may be engaged.

The report also examines the detectability of typical targets under various weather conditions for passive imagers at both IR and MMW frequencies. The analysis is limited to detection ranges of 2 km or less. The primary reason for the 2-km limitation is that MMW imagers usually have difficulty detecting typical targets at greater distances. Section 2 analyzes the relative performance of these imagers in rain, fog, snow, and clouds. Section 3 gives the frequency of occurrence of these weather conditions for various locations around the world. The locations were picked because of potential U.S. involvement and their representations of adverse weather conditions. Section 4 summarizes the report.

2. Weather Analysis

This section examines the ability of passive IR and MMW systems to detect objects under adverse conditions that are less than 2 km away. The analysis is tailored to fit the constraints imposed by the climatology database, ARL's Electro-Optical Systems Atmospheric Library 1992 (EOSAEL 92) Climatology Module (see sect. 2.1 for a description). The 2-km limitation is chosen because the mean visibility in classes 2, 8, and 12 of the EOSAEL 92 Climatology Module is usually less than 2 km, and at greater distances MMW imagers usually have difficulty resolving typical targets. Therefore, only clouds (class 20) and those classes that have a mean visibility less than 2 km, that is, fog (classes 1 and 2), rain (classes 7 and 8), and snow (classes 11 and 12) were analyzed.

The performance of a passive detection system is highly dependent on the parameters of the specific system being used, and the means of detection for IR systems is different than for MMW systems. Consequently, I did not examine IR and MMW detection in precise detail, rather, I investigated

general trends. For example, consider an unmanned air vehicle (UAV) flying at 1000 m altitude during good weather conditions but looking down through 300 m of clouds. If a cloud depth of 50 m does not allow a second-generation forward-looking infrared (FLIR) device to detect a tank with 50-percent probability but causes negligible attenuation to a passive MMW system, we assume that a tank will not be detectable with a FLIR on a UAV, but it will be detectable with a passive MMW system. This is the type of analysis done in this report.

2.1 Climatology Database—The EOSAEL 92 Climatology Module

Meteorological data are provided to the U.S. Air Force Environmental Technical Application Center by 795 stations around the world. The EOSAEL 92 Climatology Module divides these data into 74 nonoverlapping climatic regions. Each region is further divided into four time periods for the day and the four seasons. Meteorological data for a particular time of day, season, and region are provided in terms of the following classes:

Class 1 = fog, haze, and mist with visibility < 1 km.

Class 2 = fog, haze, and mist with visibility > 1, < 3 km.

Class 3 = fog, haze, and mist with visibility > 3, < 7 km.

Class 4 = fog, haze, and mist with visibility > 7 km.

Class 5 = dust with visibility < 3 km.

Class 6 = dust with visibility > 3 km.

Class 7 = drizzle, rain, and thunderstorms with visibility < 1 km.

Class 8 = drizzle, rain, and thunderstorms with visibility > 1, < 3 km.

Class 9 = drizzle, rain, and thunderstorms with visibility > 3, < 7 km.

Class 10 = drizzle, rain, and thunderstorms with visibility > 7 km.

Class 11 = snow with visibility < 1 km.

Class 12 = snow with visibility > 1, < 3 km.

Class 13 = snow with visibility > 3, < 7 km.

Class 14 = snow with visibility > 7 km.

Class 15 = no weather and absolute humidity < 10 g/m^3.

Class 16 = no weather and absolute humidity > 10 g/m^3.

Class 17 = visibility < 1 km and ceiling height < 300 m.

Class 18 = visibility < 3 km and ceiling height < 1000 m.

Class 19 = ceiling height < 300 m.

Class 20 = ceiling height < 1000 m.

Class 21 = no ceiling.

Class 22 = all conditions combined.

The data given for the classes are mean temperature, humidity, visibility, pressure, cloud height, and wind information. This limited selection of information is used to estimate how FLIRs and passive MMW systems will perform at various times and locations throughout the world. Obviously, the analysis had to be tailored to fit within the parameters of the classes of the climatology database.

2.2 Weather Analysis Method for IR Systems

The U.S. Army Night Vision and Electronic Sensors Directorate's (NVESD's) computer model Acquire provides the probability of detection versus range.* The inputs to this model are target height and length, ΔT in Kelvin, atmospheric transmittance for a 1-km path, a minimum resolvable temperature (MRT) data deck, and cycle criterion (from the Johnson criteria) [1] to perform an acquisition task such as detecting an object.

The default values of 2.3×2.3 m and 1.25 K were used for the target height and length, and ΔT, respectively. The atmospheric transmission was obtained from LOWTRAN 7, a relatively low-resolution computer code that computes atmospheric transmittance in the IR region; the data deck was obtained from the models (GEN2 for the 8- to 12-μm band and STARE for the 3- to 5-μm band) that came with NVESD's FLIR92 Thermal Imaging Systems Performance Model. The cycle criterion number used was 0.83, which is an average of the Johnson criteria for detection of a truck (0.90), M-48 tank (0.75), Stalin tank (0.75), Centurion tank (0.75), and a half track (1.0) [1].

The values of 0.83 for the Johnson criteria and 2.3×2.3 m for the target area, which were used as inputs to Acquire, are different than the Johnson criteria default value of 0.75 and the target area used by Wikner† in his MMW analysis. Obviously, the larger the target and smaller the Johnson criteria the greater the detection range. However, small changes in the Johnson criteria and target size do not quantitatively affect the detection range. This is shown in figure 1, which shows the range for 50-percent probability of detection versus visibility for the 8- to 12-μm band for three different cases: (1) Johnson, criteria = 0.83 and target area is 2.3×2.3 m,

Actually, the Acquire model gives the probability of performing a certain task such as detection or recognition versus range, where the task is defined in terms of the Johnson criteria.

†*The results from Wikner's Army Research Laboratory report, "A Prediction of 94 GHz Radiometer Performance in Various Environmental Condition for Army Applications," ARL-TR-1103, September 1996, are used in section 2.3, Weather Analysis Method for MMW Systems.*

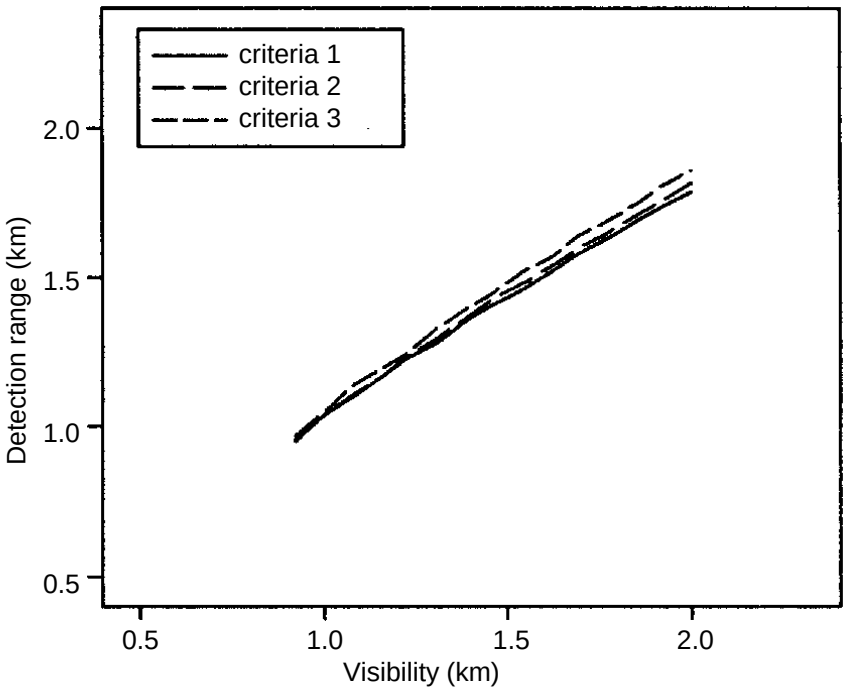

Figure 1. Detection range versus visibility in advective fog for the 8- to 12-μm band for three different cases: (1) Johnson criteria =0. 83, target is 2.3 × 2.3 m; (2) Johnson criteria = 0.75, target is 2.3 × 2.3 m (the default values); and (3) Johnson criteria = 0.83, target is 3 × 3 m.

(2) Johnson criteria = 0.75 and target area is 2.3 × 2.3 m (default values of the Acquire model), and (3) Johnson criteria = 0.83 and target area is 3 × 3 m.

At very low transmittance the Acquire model does not work. Therefore, an assumption was made that a FLIR could not detect a target with 50-percent probability or better at a distance that corresponds to a transmittance of 0.01 or less. This assumption is consistent with observations of workers in the field and the fact that the Acquire model will not work for transmittance input of approximately 0.015 or less.

The analysis for the IR propagation through cloud does not use the Acquire model; instead, the analysis uses the fact that the extinction coefficient through clouds for the 8- to 12-μm band can be modeled by [2]

$$\beta_{8\text{- to }12\text{-}\mu\text{m}} = 139\ (\text{liquid } H_2O)^{1.03}\ . \tag{1}$$

The transmittance τ is then calculated from

$$\tau = e^{-\beta x}\ , \tag{2}$$

where x is the distance over which the transmittance is calculated. The depths at which the transmittance is 1 percent for various cloud types were calculated. Because this depth is typically tens of meters, it was concluded that it is reasonable to assume that IR radiation cannot penetrate through clouds. Implicit in this conclusion is the assumption that the transmittance through clouds for the 3- to 5-μm band is no better than for the 8- to 12-μm band.

The assumptions used for the IR weather analysis are summarized in list 1.

List 1. Assumptions used for IR weather analysis.

1. MRT inputs for Acquire model were taken from STARE or GEN2 models.
2. Johnson criteria = 0.83.
3. Target area = 2.3×2.3 m^2.
4. ΔT = 1.25 K.
5. Transmittance inputs to Acquire model were obtained from LOWTRAN 7.
6. FLIR cannot detect target with 50% probability or better at distance that corresponds to transmittance of 0.01 or less.
7. Extinction coefficient through clouds for 8- to 12-μm band is given by $\beta_{8\text{- to }12\text{-}\mu m} = 139 \text{ (liquid } H_2 0)^{1.03}$.
8. Transmittance through clouds for 3- to 5-μm band is no better than for 8- to 12-μm band.

2.3 Weather Analysis Method for MMW Systems

The results of this section are taken from Wikner [3]. His assumptions are in table 1 and the results are in tables 2 and 3.

Notice that the detection ranges for the ground-to-ground and air-to-ground scenarios are different. This is due to the assumptions of a larger reflected target area (10 m^2 as opposed to 4.4 m^2) and less atmospheric attenuation for the air-to-ground system. The larger target area yields a larger fill factor η in equation (A-15) (see app). The air-to-ground path has less attenuation than the ground-to-ground path because water density decreases as altitude increases and fog only exists for part of the air-to-ground path, which is the first 500 m of altitude.

Attenuation values for widespread rain and snow were obtained from the near millimeter wave (NMMW) module that accompanies EOSAEL.

2.4 Fog Analysis

Fog is usually classified into two types, advective and radiation. Radiation fog is created when the air loses heat, usually by radiation, and becomes saturated. This type of fog generally occurs during the winter and usually fades as the sun warms the air. Advective fog is due to moist air advecting from a source (a large body of water) and coming in contact and being cooled by a cold surface. Table 4 presents some nominal characteristics of the two types of fog.*

LOWTRAN 7 was used to obtain the transmittance for a l-km path as a function of visibility for radiation and advective fog. These values, along with the required target information (Johnson criteria = 0.83; target area = 2.3×2.3 m), were inputted into the Acquire model to obtain detection range versus visibility. Figure 2 shows the detection range in radiation fog of a second-generation FLIR in the 8- to 12-μm band versus visibility;

**Taken from "Millimeter Wave Engineering and Applications," Bhartia and Bahl. The identical table is in "Millimeter Wave Radar," Stephen L. Johnson ed., Artech House, 1980, and came from "Study of Atmospheric Propagation Factors for 70 GHz Energy," Stanford Research Institute, 26 August 1969 (supplied by SRI under Nordon PO 0016146—not available for distribution).*

Table 1. MMW assumptions.

Item	Assumed value
Frequency	94 GHz
Target size	$3 \times 3 \times 6$ m^3
ΔT	2 K
Depression angle	60°
Antenna beamwidth	3.1 mrad

Table 2. MMW detection range, ground-to-ground scenario.

Environmental condition	Detection range (km)
100-m visibility fog	4.2
24-m visibility fog	1.8
Stratus clouds, 1000 to 2000 m	>5.0
Cumulus congestus clouds, 1000 to 2000 m	2.9
Drizzle, 1 mm / hr, cumulus congestus	2.1
Steady rain, 5 mm / hr, cumulus congestus	1.3
Heavy rain, 10 mm / hr, cumulus congestus	<0.5

Table 3. MMW detection range, air-to-ground scenario.

Environmental condition	Detection range (km)
100-m visibility fog	>5.0
24-m visibility fog	4.6
Stratus clouds, 1000 to 2000 m	>5.0
Cumulus congestus clouds, l000 to 2000 m	3.1
Drizzle, 1 mm / hr, cumulus congestus	2.2
Steady rain, 5 mm / hr, cumulus congestus	1.3
Heavy rain, 10 mm / hr, cumulus congestus	<0.5

Table 4. Fog characteristics.

Characteristic	Radiation (inland) fog	Advective (coastal) fog
Average drop diameter	10 µm	20 µm
Typical drop-size range	5–35 µm	7–65 µm
Liquid water content	0.11 g / m^3	0.17 g / m^3
Droplet concentration	200 / cm^3	40 / cm^3
Visibility	100 m	200 m

figure 3 shows the detection range in radiation fog of a staring FLIR in the 3- to 5-µm band versus visibility. Figure 4 shows the equivalent information for advective fog. Note that advective fog affects the 3- to 5-µm and 8- to 12-µm bands equally, while radiation fog has a much greater effect on the 3- to 5-µm band.

Because the Acquire model does not work when the transmittance goes below 0.015, another method was needed to estimate the detection range for low atmospheric transmissions. The maximum detection range was chosen to be the distance at which transmittance equals 0.01. Transmittance is plotted as a function of visibility in figures 5 and 6 for a 1-km path for advective and radiation fog, respectively. The graphs can then be used to determine the visibility for which an object cannot be detected.

Figure 2. Detection range as function of visibility for second-generation FLIRs in radiation fog for 8- to 12-μm band.

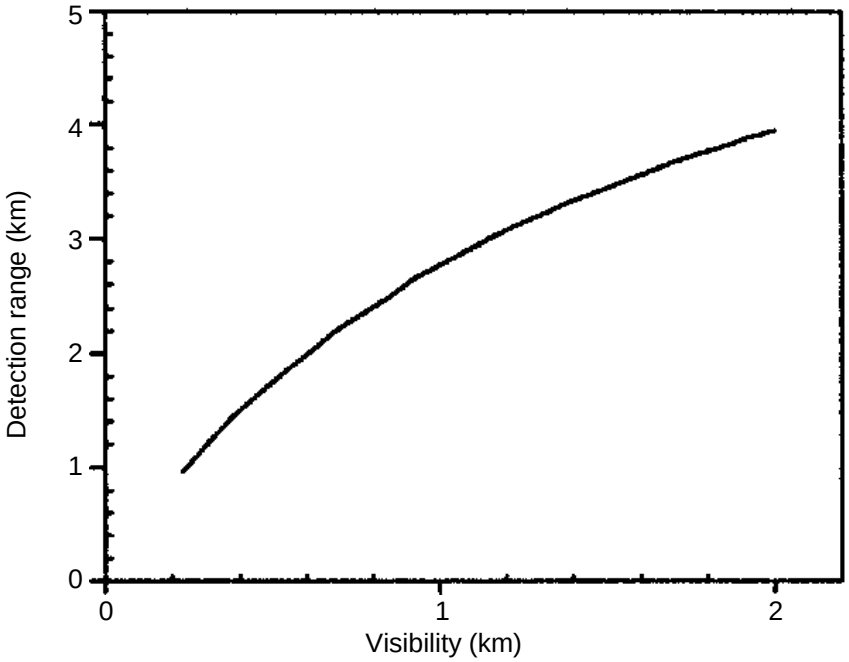

Figure 3. Detection range as function of visibility for staring FLIR in radiation fog for 3- to 5-μm band.

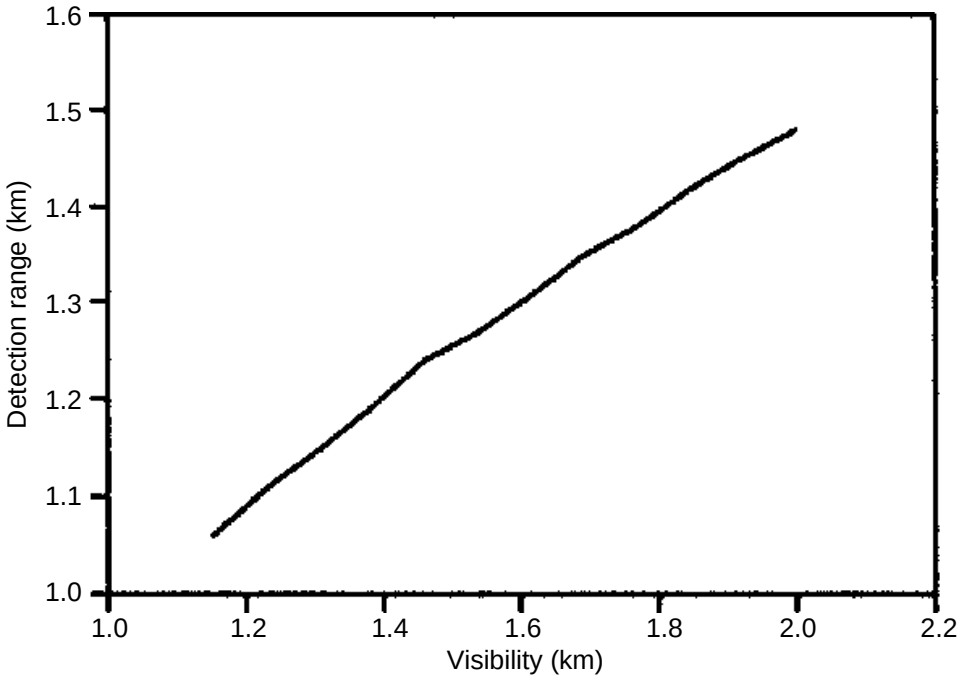

Figure 4. Detection range as function of visibility for 3- to 5-μm and 8- to 12-μm FLIRs in advective fog.

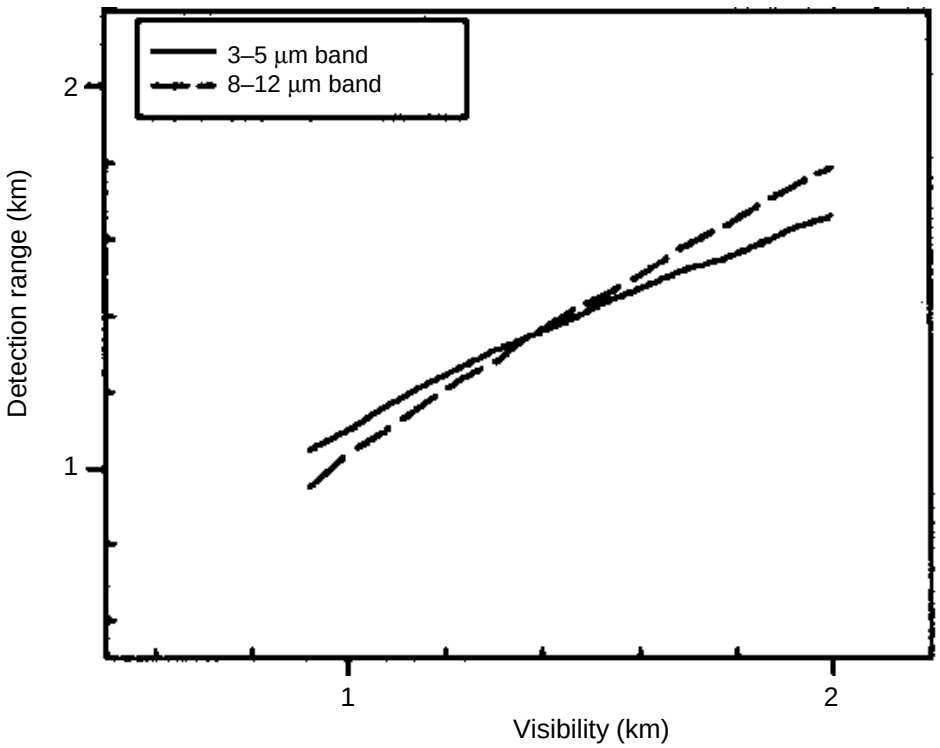

Figure 5. Transmittance as function of visibility* for 1-km path in advective fog.

**The data came from LOWTRAN 7. LOWTRAN 7 uses the meteorological range as an input rather than visibility of an observer. The data meteorological range can be estimated by "meteorological range = (1.3 ± 0.3) × visibility of an observer." The values on the x-axis were determined from the meteorological range/ 1.3.*

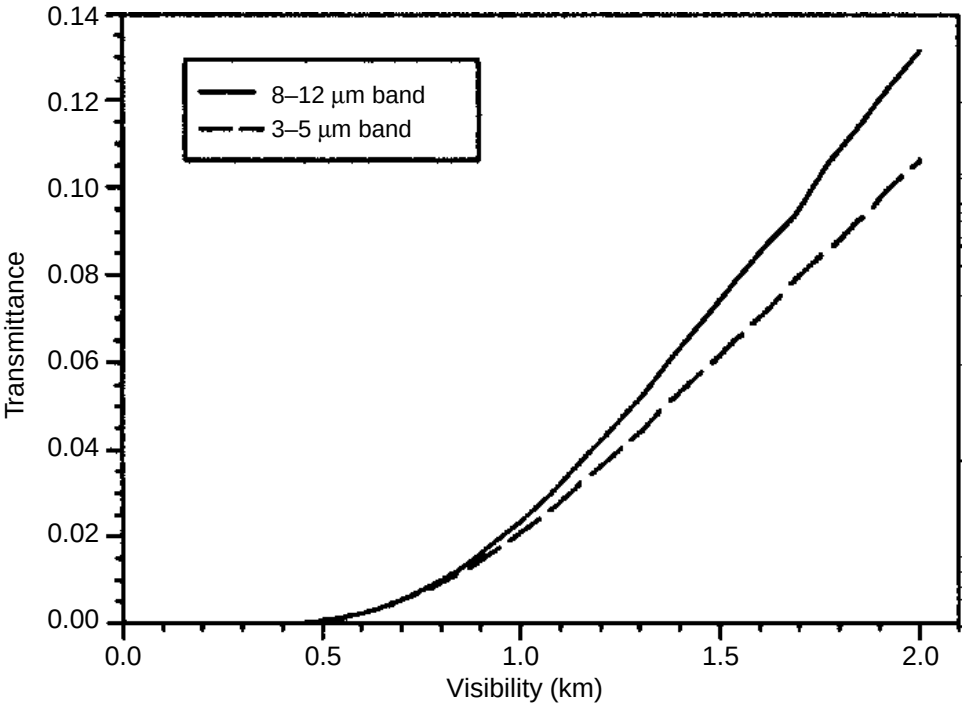

Figure 6. Transmittance as function of visibility for 1-km path in radiation fog.

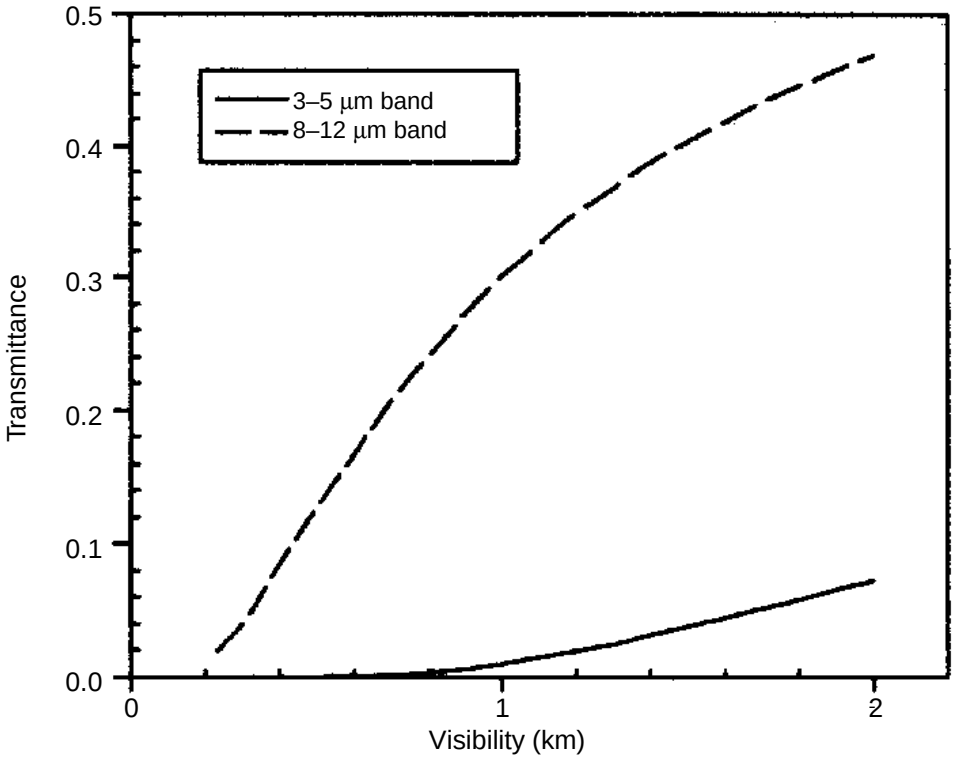

For example, from figure 5, when the visibility is approximately 1.8 km, the transmittance for a 1-km path is approximately 0.1; this implies the transmittance for a 2-km path is approximately 0.01. Therefore, when the visibility in advective fog becomes less than 1.8 km, an IR system will not be able to detect an object beyond 2 km. This information can then be used to determine when a system with MMW will be able to detect a target, while a system with only IR will not be able to detect a target. This method gives an upper limit to the detection range. For example, according to figure 4, which is based on the MRT detection method, the detection range of a FLIR through advective fog with 1.8 km visibility would be 1.6 km, not 2 km.

For advective fog, the IR detection range is approximately equal to the visibility of the fog (for an advective fog with 2-km visibility the 50-percent probability detection range in the 3- to 5-μm band is 1.7 km and for the 8- to 12-μm band it is 1.8 km). For radiation fog, the IR detection range is less than the visibility of the fog for the 3- to 5-μm band (for a radiation fog with 2-km visibility the 50-percent probability detection range in the 3- to 5-μm band is 1.5 km) and much better than the visibility of the fog for the 8- to 12-μm band. (According to figure 2, the 50-percent probability detection range in the 8- to 12-μm band for 2-km visibility radiation fog is 4 km, and the detection range does not get below 2 km until the visibility of the fog goes down to around 600 m.)

For MMW systems, table 3 indicates that fog is not a factor for air-to-ground scenarios at a distance of 2 km and, according to table 2, only a factor at 2 km when the visibility is around 25 m. Because 25-m visibility fog is rare, we can generally say that for 2-km air-to-ground or ground-to-ground scenarios, MMW systems are not fog-limited.

In conclusion, for ranges up to 2 km, MMW systems are not limited by fog; advective fog limits IR systems, radiation fog limits 3- to 5-μm band systems and limits 8- to 12-μm band systems when the visibility is less than 600 m.

2.5 Rain Analysis

The approximate atmospheric attenuations for IR in rain are

- drizzle, 1 dB/km,
- widespread, 3 dB/km, and
- thunderstorm, 20 dB/km.

Therefore, the IR detection range through rain will exceed 2 km except in thunderstorms.

Figure 7 shows attenuation in widespread rain for a 1-km path as a function of rain rate for 35 and 94 GHz, as determined from the NMMW model. A comparison of the MMW atmospheric attenuations in figure 7

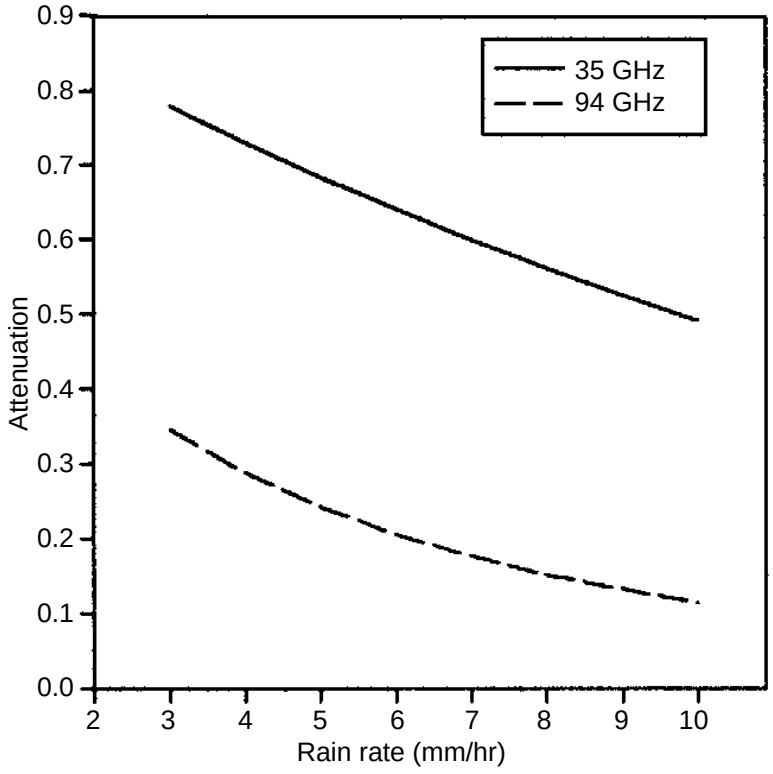

Figure 7. Attenuation in widespread rain as function of rain rate for 35 and 94 GHz for 1-km path.

(1–3 dB for 35 GHz and 5–10 dB for 94 GHz) with IR atmospheric attenuations (3 dB) shows that there is no advantage of MMW propagation over IR propagation in widespread rain.

Performance in thunderstorms is very poor for passive MMW systems, due to the large particle size and the higher radiometric sky temperature that accompanies thunderstorms. Tables 2 and 3 indicate that widespread rain can have a significant effect on performance of a MMW system. Because passive MMW systems do not appear to have an advantage over passive IR systems in widespread rain, further rain analysis is unnecessary for the purposes of this report.

2.6 Snow Analysis

IR attenuation in snow can be calculated if the snow rate, wind velocity, and particle size distribution and water content of the snow crystals are known. However, the climatology database does not give enough information to determine these factors. A further complication is that the climatology database does not separate snow from snow and fog, and snow and rain, thus, it is not possible to tell the frequency of occurrence of only snow from the climatology database.

Snow is very difficult to analyze because its properties change according to the location, temperature, wind velocity, and other factors. The NMMW computer model will generate attenuation for a given MMW frequency as a function of equivalent rain rate; this is shown in figure 8.* As a rule of thumb, meteorologist use a ratio of 10:1 for comparing snowfall rate to equivalent rain rate; that is, a snowfall rate of 20 mm / hr equals an equivalent rain rate of 2 mm / hr. This rule of thumb also varies according to location. For example, in the winter in Bosnia, a ratio of 12:1 to 15:1 should be used, while along a coast a ratio of 8:1 is more appropriate.† Figure 8 shows transmission versus snow equivalent rain rate. Notice that figure 8 indicates that a nominal snow equivalent rain rate of 1 mm / hr gives very little attenuation at 35 GHz and only 0.5 dB loss at 95 GHz.

Typically, snow attenuation is given as a function of airborne snow mass concentration. Figure 9 gives the correlation of mass concentration (g / m^{-3}) and snow rate (mm / hr) for snow that occurred during the 31 January 1982 snow storm at the Camp Ethan Allen Training Center of the Vermont National Guard in Jericho, Vermont.

Personnel taking measurements in snow have observed that MMW can frequently see through snow when IR cannot. Table 5, which gives measured attenuation values for snow [4], makes this statement quantitative.

**The assumptions used in the model were as follows: temperature = –8.6°C, relativity humidity = 97%, pressure = 1015 mbar, path length = 1 km.*

†Generally, overland and in a colder climate snow has a low water content, while along a coast snow has a higher water content.

Figure 8. Transmittance versus snow rate (mm/hr rain equivalent) for 1-km path.

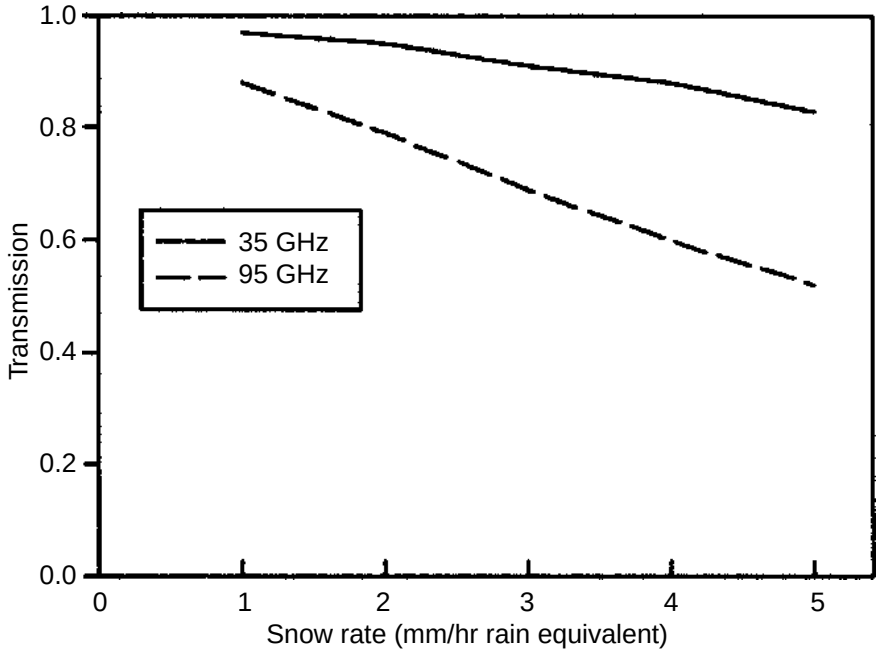

According to figure 9, a mass concentration of 0.3 g/m^{-3} corresponds to a snow rate of 0.77 mm/hr. When the value of 0.77 mm/hr is put into the NMMW computer code, an attenuation of 0.5 is obtained for 96 GHz for a 1-km path, which is the measured value given in table 5. Therefore, the NMMW program and the measured data are consistent.

The measured data in table 5 imply that for a snow mass concentration of 0.3 g/m^{-3}, the IR detection range is limited to approximately 1 and 1.5 km for 10 and 4 μm, respectively, while a passive MMW system should be able to detect a metal target at 2 km. Even though it is impossible to use the EOSAEL 92 Climatology Module to determine where and when MMW detection will outperform IR detection, the above analysis shows the advantage of a passive MMW system over a passive IR system for a snow mass concentration of 0.3 g/m^{-3}.

2.7 Cloud Analysis

Class 20 of the climatology database gives the percentage of occurrences of ceiling height below 1 km. Typical characteristics for the four types of clouds with bases below 1 km are given in table 6 [5].

It is said that IR cannot "see" through clouds. This can be made quantitative by calculating the extinction coefficient for the 8- to 12-μm band. We use equations (1) and (2) to calculate the range x where the transmittance is 0.01, obtaining

$$x = -\frac{\ln(0.01)}{139\,(\text{liquid } H_2 0)^{1.03}} \approx -\frac{\ln(0.01)}{139\,(\text{liquid } H_2 0)}\ \text{km} \quad . \tag{3}$$

Figure 9. Correlation of mass concentration (*M*) and snow rate (*P*).

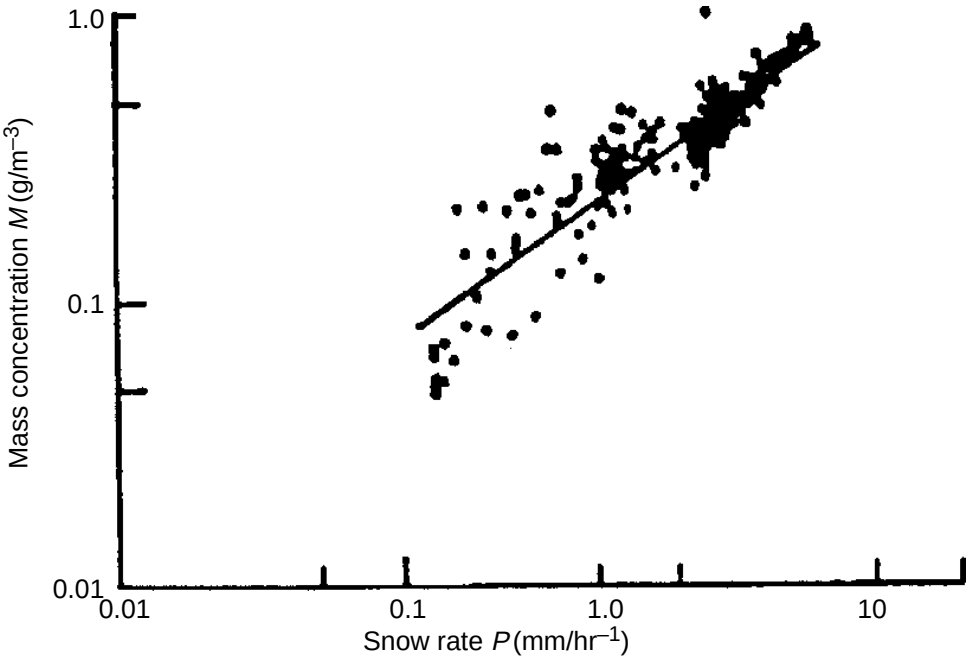

Table 5. Measured values of attenuation in snow for snow mass concentration of 0.3 g/m^{-3}.

Wavelength	Attenuation (dB / km)
0.55 μm	13
4 μm	12
10 μm	20
3.13 mm (96 GHz)	0.5

Table 6. Cloud characteristics.

	Altitude		
Cloud type	Bottom	Top	Liquid water content (g / m^{-3})
Cumulus	660	3500	0.50–1.00
Stratocumulus	150	660	0.30–0.60
Nimbostratus	660	2700	0.60–0.70
Stratus	160	2000	0.15–0.30

Equation (3) can then be used to determine the cloud depths at which the transmittance is 1 percent. This and the liquid water content values used in equation (3) are shown in table 7. Because the wavelength for the 3- to 5-μm band is shorter than that for the 8- to 12-μm band, the detection ability of a FLIR through clouds in the 3- to 5-μm band is expected to be worse.

Because the depths of the clouds shown in table 6 are usually at least several hundred meters, a system at 1 km or greater altitude would have to penetrate at least several hundred meters of cloud to detect targets on the ground. Therefore, considering the inability of IR to penetrate clouds, we can assume that class 20 (the percentage of times ceiling height is below 1000 m) gives the percentage of time an air-to-ground IR system flying at an altitude of 1 km or higher will not be able to detect an object on the ground with 50-percent probability. Table 3 indicates that an air-to-ground MMW system can "see through" several kilometers of cloud unless there is rain heavier than a drizzle. Therefore, the analysis in this section concludes

that a passive IR system cannot detect a target through clouds from an altitude of l km or higher, while a passive MMW system can detect a target through clouds at a distance of 2 km unless there is rain heavier than a drizzle. In terms of the EOSAEL 92 Climatology Module, this means that class 20 gives the percentage of times that cloud cover will prevent an IR air-to-ground system operating at 1 to 2 km altitude from detecting targets, and class 7 (the percentage of times that drizzle, rain, and thunderstorms with visibility below 1 km occur) gives the percentage of times that cloud cover will prevent a MMW air-to-ground system operating at 1 to 2 km altitude from detecting targets. Therefore, the percentage of times that an air-to-ground systems utilizing MMW will detect targets while one utilizing IR will not is given by class 20 minus class 7.

2.8 Summary

Table 8 presents a summary of the weather conditions that result in an advantage of passive MMW system over passive IR systems. Because we used the EOSAEL 92 Climatology Module to determine when these conditions occur, the appropriate EOSAEL 92 Climatology Module classes are given.

Table 7. IR cloud depth calculation results.

Cloud type	Liquid water content (g/m^{-3})	Depth at which transmittance = 1% (m)
Cumulus	0.75	44
Stratocumulus	0.45	73
Nimbostratus	0.65	51
Stratus	0.23	144

Table 8. Summary of advantages of passive MMW system over passive IR system.

Condition	Result	Appropriate EOSAEL 92 climatology class
Rain	No advantage	NA
Advective fog	Large advantage	1 and 2
Radiation fog	Large advantage over 3- to 5-μm band	1 and 2
	Advantage over 8- to 12-μm band when visibility ≤0.5 m	1
Clouds	Large advantage	20 minus 7
Snow	Advantage	11 and 2

3. Fog, Snow, and Cloud Occurrences for Selected Areas

We have shown that a passive MMW system can have a significant advantage over a FLIR in clouds and fog, and, to a lesser extent, in falling snow. This section examines the frequency of occurrence of those weather conditions for certain locations around the world for each of the four seasons during the morning (0300-0900), midday (1000-1400), evening (1500-1900), and night (2000-0200). The day is divided into four time periods to take advantage of the predictable diurnal variation of some weather aspects. For example, fog is more prevalent in the morning hours than the evening hours. The weather information is extracted from the EOSAEL 92 Climatology Module.

For reasons mentioned earlier, this section is only concerned with those classes of the EOSAEL 92 Climatology Module that have a mean visibility below 2 km; that is, classes 1, 2, 11, 12, and 20. Tables listed in this section provide the percentage of times for occurrence of fog, classes 1 and 2; the percentage of times for occurrences of snow, classes 11 and 12; the percentage of times the cloud height is below 1 km, class 20; and the percentage of times the cloud height is below 1 km minus the percentage of times drizzle, rain, and thunderstorms with visibility below 1 km occur, class 20 minus class 7. (Class 7 has to be subtracted from class 20 because a passive MMW system does not detect targets well during steady rain or thunderstorms.)

3.1 Korea

Korea is a peninsula in East Asia between the Yellow Sea and the Sea of Japan. Its primary mountains are the Taeback Range [6]. (See fig. 10.) This range is oriented north to south along the east coast. Another range, the Sobaek, extends southwestward from the center of the Taeback Range. The Taeback and Sobaek mountain ranges divide Korea into the west, east coast, and southern regions. A third mountain range, Hangyong, runs northeast to southwest in the northern part of Korea. Its climate is similar to the Jilin Kirin province of China.

3.1.1 Korea East Coast

Tables 9 through 11 provide cloud and fog data from the EOSAEL 92 Climatology Module. The data are divided into morning, midday, evening, and night times for each of the four seasons for the Korea East Coast region shown in figure 10. Table 12 provides data on snow with mean visibility below 2 km, averaged throughout the day during the four seasons.

Figure 10. Regions of Korea taken from climatology database.

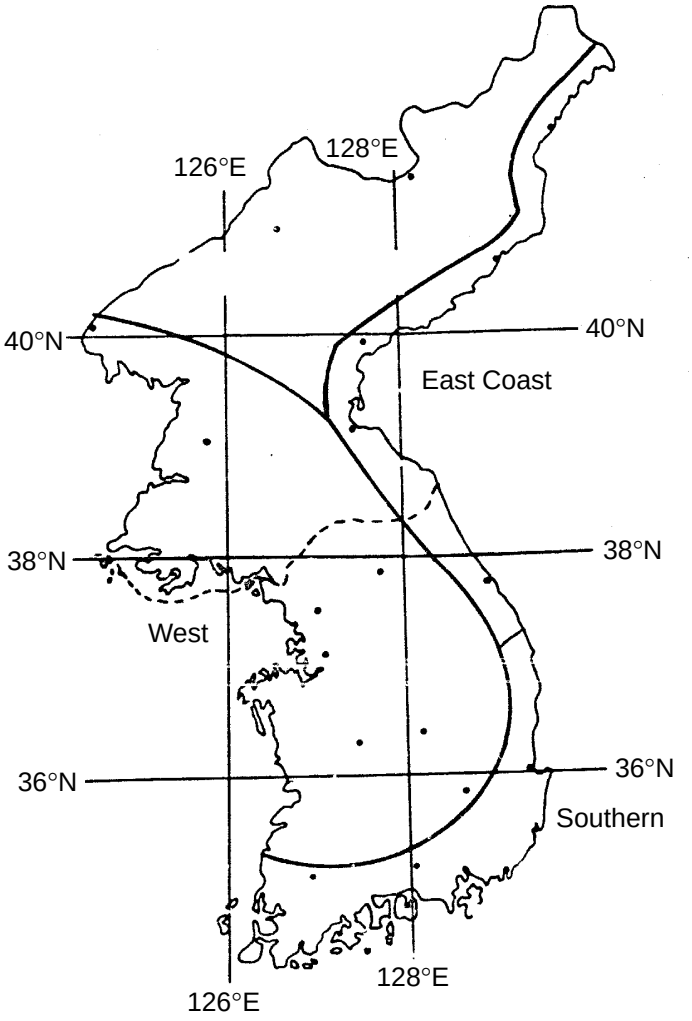

Table 9. Percentage of times fog with mean visibility ≤ 2 km occurs in Korea East Coast.

Time of day	Winter	Spring	Summer	Autumn
0300–0900	4.6	10.3	13.1	5.7
1000–1400	2.5	5.3	7.8	1.9
1500–1900	1.4	3.9	4.6	1.1
2000–0200	1.1	5.0	5.1	0.8

Table 10. Percentage of times cloud ceiling < 1 km occurs in Korea East Coast.

Time of day	Winter	Spring	Summer	Autumn
0300–0900	22.9	29.8	58.7	31.5
1000–1400	21.9	28.3	53.5	31.5
1500–1900	23.5	31.0	55.4	33.2
2000–0200	21.7	27.3	56.4	29.3

Table 11. Percentage of times cloud ceiling < 1 km minus percentage of times rain with visibility < 1 km occurs in Korea East Coast.

Time of day	Winter	Spring	Summer	Autumn
0300–0900	22.8	29.1	57.2	31.4
1000–1400	21.8	28.0	52.8	31.3
1500–1900	23.5	30.5	54.7	33.1
2000–0200	21.6	26.7	55.6	29.1

Table 12. Percentage of times snow with mean visibility ≤ 2 km occurs in Korea East Coast.

Winter	Spring	Summer	Autumn
2.5	0.5	0.0	0.1

3.1.2 South Korea

Tables 13 through 15 provide cloud and fog data obtained from the EOSAEL 92 Climatology Module. The data are divided into morning, midday, evening, and night times for each of the four seasons for the South Korea region shown in figure 10. The only significant frequency of occurrences of snow for South Korea is during the winter and it occurs with mean visibility below 2 km 0.4 percent of the time.

3.1.3 West Korea

Tables 16 through 18 provide cloud and fog data obtained from the EOSAEL 92 Climatology Module. The data are divided into morning, midday, evening, and night times for each of the four seasons for the West Korea region shown in figure 10. Table 19 provides data on snow with mean visibility below 2 km, averaged throughout the day during the four seasons.

3.1.4 Summary

Fog is most prevalent during the morning hours in the summer and in the Korean East Coast, which has a frequency of occurrence of 13 percent during the summer morning hours. Table 20 presents a summary of the percentages of occurrence of fog during the morning hours for the four seasons averaged over all three regions. We have also shown that Korea has a significant amount of cloud coverage. Table 21 presents a summary of these results averaged throughout the day.

3.2 Former Yugoslavia Area

The EOSAEL 92 Climatology Module divides the regions in and around the former Yugoslavia [7] into the regions shown in figure 11. Bosnia is located in region M, which is called the European Dinaric Alps.

Table 13. Percentage of times fog with mean visibility ≤ 2 km occurs in South Korea.

Time of day	Winter	Spring	Summer	Autumn
0300–0900	1.3	2.1	3.6	3.0
1000–1400	0.2	0.2	0.8	0.2
1500–1900	0.0	0.1	0.7	0.1
2000–0200	0.3	0.2	0.6	0.2

Table 14. Percentage of times cloud ceiling < 1 km occurs in South Korea.

Time of day	Winter	Spring	Summer	Autumn
0300–0900	25.4	28.2	43.4	24.3
1000–1400	21.0	27.2	40.3	22.8
1500–1900	23.3	26.9	35.5	23.3
2000–0200	27.5	27.5	39.0	24.7

Table 15. Percentage of times cloud ceiling < 1 km minus percentage of times rain with visibility < 1 km occurs in South Korea.

Time of day	Winter	Spring	Summer	Autumn
0300–0900	25.4	28.1	43.1	24.2
1000–1400	20.9	27.1	39.9	22.8
1500–1900	23.3	26.8	35.3	23.3
2000–0200	27.5	27.5	38.9	24.7

Table 16. Percentage of times fog with mean visibility ≤ 2 km occurs in West Korea.

Time of day	Winter	Spring	Summer	Autumn
0300–0900	7.4	5.9	8.7	10.0
1000–1400	5.3	2.3	2.4	2.5
1500–1900	2.1	1.4	1.8	0.7
2000–0200	2.7	2.4	3.2	1.9

Table 17. Percentage of times cloud ceiling < 1 km occurs in West Korea.

Time of day	Winter	Spring	Summer	Autumn
0300–0900	25.5	24.5	44.7	25.8
1000–1400	23.0	23.2	40.4	22.1
1500–1900	23.3	23.0	37.1	21.8
2000–0200	23.8	21.5	35.5	20.2

Table 18. Percentage of times cloud ceiling < 1 km minus percentage of times rain with visibility < 1 km occurs in West Korea.

Time of day	Winter	Spring	Summer	Autumn
0300–0900	25.4	24.2	43.9	25.1
1000–1400	22.9	23.0	39.9	22.0
1500–1900	23.1	22.8	36.7	21.7
2000–0200	23.7	21.2	35.0	20.1

Table 19. Percentage of times snow with mean visibility ≤ 2 km occurs in West Korea.

Winter	Spring	Summer	Autumn
1.3	0.2	0.0	0.1

Table 20. Percentage of times fog occurs during morning averaged over three regions in Korea.

Time of day	Winter	Spring	Summer	Autumn
0300–0900	4	6	8	6

Table 21. Percentage of times cloud ceiling < 1 km occurs for areas in Korea.

Regions	Winter	Spring	Summer	Autumn
Korea East Coast	23	29	56	31
South Korea	24	27	40	24
West Korea	24	23	39	22

Figure 11. Regions from climatology database that contain or are near Bosnia. Dotted line shows former Yugoslavia; Bosnia is identified by M.

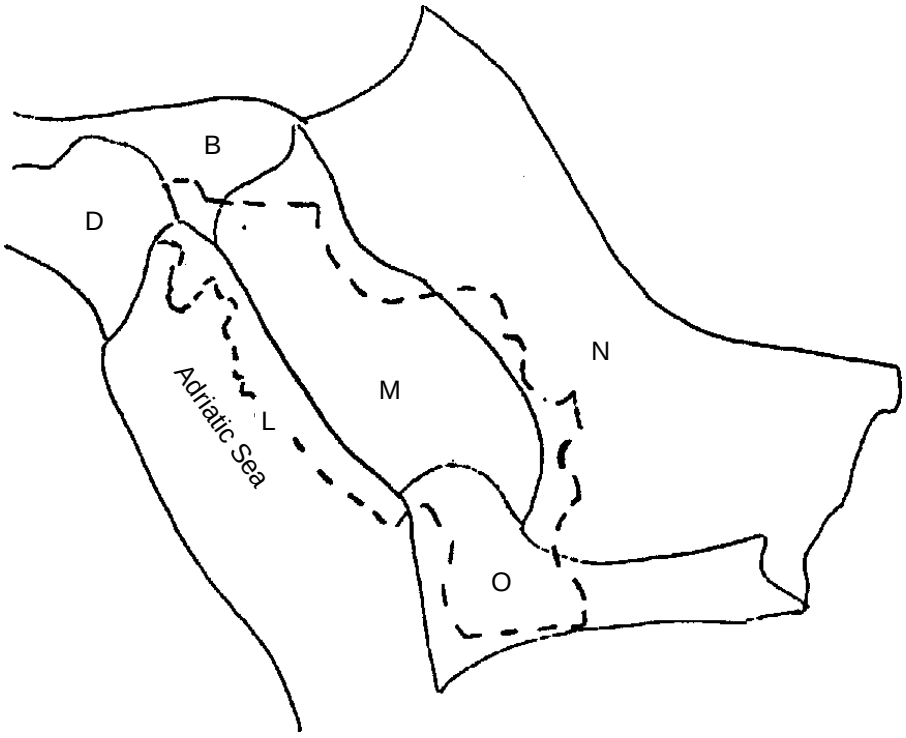

B Highlands
D Alpine
L Adriatic Alps
M Dinaric Alps
N Balkan Plains
O Balkan Highland

3.2.1 Dinaric Alps

The Dinaric Alps are mainly in the former Yugoslavia. (See fig. 11.) This mountain range has an average height of 1500 m and several peaks above 2500 m. Tables 22 through 25 provide weather data obtained from the EOSAEL 92 Climatology Module. The data are divided into morning, midday, evening, and night times for each of the four seasons for the Dinaric Alps region. Note that the mean visibility given in table 23 is for less than 300 m. Because of the prominence of adverse weather conditions in the morning during the autumn and winter, table 26 is devoted to that time.

3.2.2 Balkan Highlands

The Balkan Highlands [7] consist of elevated regions of former southeast Yugoslavia, eastern Albania, northern Greece, and western Bulgaria. The principal mountain ranges are the Balkan and the Rhodop. Visibility is poor in the mountains during most of the winter, with mountain peaks and ridges often obscured by clouds. Tables 27 through 30 give the percentages of times for occurrences of various weather conditions for the region Balkan Highlands (region O in fig. 11). Note that the mean visibility given in table 28 is for less than 200 m. Because of the prominence of adverse weather conditions in the autumn and winter, table 31 gives the weather statistics for the Balkan Highlands during the autumn and winter from 0300 to 1400, averaged over the whole day.

3.2.3 Balkan Plains

The lower elevation areas of Bulgaria, Romania, Hungary, and the former Yugoslavia form the Balkan Plains region [7] (region N in fig. 11). The lower elevation areas in Bulgaria are the Danube Plateau and the Maritsa Valley. In Romania, the area south of the Transvanian Alps is a flat plain, and the southeastern part of Romania is an area of low-lying marshes. Most of Hungary consists of the Carpathian Basin. The Balkan Plains portion of the former Yugoslavia is the border area it shares with Hungary, Romania, and Bulgaria. The continental polar anticyclones from the former Soviet Union cause low winter temperatures. Tables 32 to 35 give the percentage of times for the occurrence of various weather conditions for the Balkan Plains region. Note that the mean visibility given in table 33 is for less than 450 m and the relatively high percentage of times the cloud ceiling is less than 1 km especially during the winter.

3.2.4 Adriatic Alps

The Adriatic Alps region [7] is between the Apennines, which protect eastern Italy from eastward moving storms, and the former Yugoslavian side of the Adriatic Sea. (See region L in fig. 11.) Tables 36 to 38 give the percentage of times for the occurrence of various weather conditions for this region.

Table 22. Percentage of times fog with mean visibility ≤ 2 km occurs in Dinaric Alps.

Time of day	Winter	Spring	Summer	Autumn
0300–0900	22.8	10.3	14.7	25.2
1000–1400	19.7	4.4	3.9	12.2
1500–1900	13.7	2.1	2.4	6.4
2000–0200	18.2	5.6	7.1	11.4

Table 23. Percentage of times fog with mean visibility < 300 m occurs in Dinaric Alps.

Time of day	Winter	Spring	Summer	Autumn
0300–0900	13.1	6.7	10.0	18.1
1000–1400	8.8	2.7	3.6	6.3
1500–1900	5.2	1.8	2.3	3.5
2000–0200	10.3	5.0	6.6	8.3

Table 24. Percentage of times cloud ceiling < 1 km occurs in Dinaric Alps.

Time of day	Winter	Spring	Summer	Autumn
0300–0900	45.7	29.7	26.1	41.9
1000–1400	40.4	26.2	23.6	33.1
1500–1900	35.5	22.3	18.2	27.3
2000–0200	43.2	28.8	24.3	33.1

Table 25. Percentage of times cloud ceiling < 1 km minus percentage of times rain with visibility < 1 km occurs in Dinaric Alps.

Time of day	Winter	Spring	Summer	Autumn
0300–0900	45.1	29.3	25.0	41.0
1000–1400	39.6	25.9	22.4	32.5
1500–l900	34.7	22.1	17.1	26.8
2000–0200	42.6	28.4	22.8	32.4

Table 26. Weather statistics for Dinaric Alps from 0300–0900 during autumn and winter.

	Percentage of occurrence	
Condition	Autumn	Winter
Cloud ceiling ≤ 1 km	42	46
Fog with visibility ≤ 1 km	18	13
Fog with mean visibility ≤ 2 km	25	23
Snow with visibility ≤ 1 km	1	2
Snow with mean visibility ≤ 2 km	2	6

Table 27. Percentage of times fog with mean visibility ≤ 2 km occurs in Balkan Highlands.

Time of day	Winter	Spring	Summer	Autumn
0300–0900	20.0	12.0	11.9	16.2
1000–1400	18.5	1.5	11.2	13.6
1500–1900	13.9	8.9	10.0	10.9
2000–0200	18.3	15.2	15.9	16.4

Table 28. Percentage of times fog with mean visibility ≤ 200 m occurs in Balkan Highlands.

Time of day	Winter	Spring	Summer	Autumn
0300–0900	16.3	11.2	11.0	13.8
1000–1400	14.0	10.9	10.7	10.9
1500–1900	10.6	8.8	9.9	9.7
2000–0200	16.1	15.1	15.8	15.6

Table 29. Percentage of times cloud ceiling < 1 km occurs in Balkan Highlands.

Time of day	Winter	Spring	Summer	Autumn
0300–0900	36.0	26.0	18.2	26.8
1000–1400	33.8	29.8	27.2	28.0
1500–1900	29.7	26.8	24.7	25.1
2000–0200	35.5	31.1	25.2	27.5

Table 30. Percentage of times cloud ceiling < 1 km minus percentage of times rain with visibility < 1 km occurs in Balkan Highlands.

Time of day	Winter	Spring	Summer	Autumn
0300–0900	36.0	25.5	16.6	25.8
1000–1400	33.4	28.7	24.7	26.8
1500–1900	29.4	25.7	22.6	24.0
2000–0200	35.5	29.9	22.3	26.3

Table 31. Weather statistics for the Balkan Highlands from 0300–1400 during autumn and winter.

Condition	Percentage of occurrence	
	Autumn	Winter
Cloud ceiling ≤ 1 km	27	34
Fog with mean visibility ≤ 200 m	13	14
Fog with mean visibility ≤ 2 km	14	18
Snow with visibility ≤ 1 km	2	6
Snow with mean visibility ≤ 2 km	3	7

Table 32. Percentage of times fog with mean visibility ≤ 2 km occurs in Balkan Plains.

Time of day	Winter	Spring	Summer	Autumn
0300–0900	20.4	7.2	4.4	16.9
1000–1400	19.5	3.0	0.2	8.7
1500–1900	15.3	1.5	0.1	6.0
2000–0200	17.2	2.7	0.8	8.8

Table 33. Percentage of times fog with mean visibility < 450 m occurs in Balkan Plains.

Time of day	Winter	Spring	Summer	Autumn
0300–0900	10.7	3.2	1.9	9.5
1000–1400	8.1	0.9	0.0	3.1
1500–1900	5.3	0.3	0.0	1.7
2000–0200	8.7	1.2	0.3	4.4

Table 34. Percentage of times cloud ceiling < 1 km occurs in Balkan Plains.

Time of day	Winter	Spring	Summer	Autumn
0300–0900	40.7	22.2	12.5	27.9
1000–1400	37.5	22.9	13.0	25.7
1500–1900	32.7	17.9	9.9	21.1
2000–0200	39.1	22.1	11.9	25.0

Table 35. Percentage of times cloud ceiling < 1 km minus percentage of times rain with visibility < 1 km occurs in Balkan Plains.

Time of day	Winter	Spring	Summer	Autumn
0300–0900	39.8	21.9	12.4	27.3
1000–1400	36.5	22.7	13.0	25.1
1500–1900	31.8	17.8	9.8	20.6
2000–0200	38.2	21.9	11.8	24.5

Table 36. Percentage of times fog with mean visibility ≤ 2 km occurs in Adriatic Alps.

Time of day	Winter	Spring	Summer	Autumn
0300–0900	5.4	4.4	1.5	6.2
1000–1400	4.1	1.8	0.2	2.3
1500–1900	3.7	1.9	0.4	3.1
2000–0200	4.1	2.0	0.5	3.6

Table 37. Percentage of times cloud ceiling < 1 km occurs in Adriatic Alps.

Time of day	Winter	Spring	Summer	Autumn
0300–0900	13.0	9.2	3.1	9.9
1000–1400	14.5	10.5	3.9	10.6
1500–1900	13.9	9.3	3.7	9.8
2000–0200	12.2	7.4	2.3	8.2

Table 38. Percentage of times cloud ceiling < 1 km minus percentage of times rain with visibility < 1 km occurs in Adriatic Alps.

Time of day	Winter	Spring	Summer	Autumn
0300–0900	12.9	9.1	3.1	9.9
1000–1400	14.4	10.4	3.9	10.5
1500–1900	13.6	9.2	3.7	9.7
2000–0200	12.1	7.3	2.3	8.2

3.2.5 Summary

With the exception of the Adriatic Sea area, the regions in and around Bosnia have a relatively high percentage of times that fog occurs. In these regions (Dinaric Alps, Balkan Plains, and Balkan Highlands) during the winter, dense fog occurs around 11 percent of the time and fog with mean visibility less than or equal to 2 km occurs around 18 percent of the time. For the other seasons fog is significantly more prevalent during the morning hours. Table 39 shows the percentage of times that dense fog and fog that has a visibility less than or equal to 2 km occur during the morning hours averaged over the three regions. Table 40 shows the percentage of times that a cloud ceiling below 1 km occurs for regions in and around Bosnia.

Table 39. Percentage of times fog occurs from 0300–0900 for regions in and around Bosnia.

Condition	Winter	Spring	Summer	Autumn
Dense fog	13	7	8	14
Fog with mean visibility ≤ 2 km	21	10	10	19

Table 40. Percentage of times cloud ceiling < 1 km occurs for regions in and around Bosnia.

Regions	Winter	Spring	Summer	Autumn
Dinaric Alps	41	27	23	34
Balkan Highlands	34	28	24	27
Balkan Plains	37	21	12	29
Adriatic Alps	13	9	3	10

3.3 Germany

Germany, in central Europe, is bordered by nine countries: Denmark to the north, Poland and the former Czechoslovakia* to the east, Switzerland and Austria to the south, and France, Luxembourg, Belgium, and the Netherlands to the west. Germany is basically within three regions dealt with by the climatology database: the Lowlands (A), the Highlands (B), and the Rhine Valley (C), as shown in figure 12.†

The German Highlands was of great concern during the cold war. The Fulda Gap and the Hof Corridor, which are in the Highlands, and the Gottingen Corridor, which borders on the Lowlands and Highlands, were considered as three possible major invasion routes from the former Warsaw Pact countries. Because of Germany's central location in Europe and the previous concern about major invasion routes there, the adverse weather conditions are examined in the Lowlands (tables 41 through 44), the Highlands (tables 45 through 48), and the Rhine Valley (tables 49 through 52).

3.3.1 Summary

For the areas in and around Germany (the Lowlands, the Highlands, and the Rhine Valley), during the winter dense fog occurs around 6 percent of the time, and fog with mean visibility less than or equal to 2 km occurs around 15 percent of the time. Fog is most prevalent during the morning hours. Table 53 shows an average of the percentage of time that fog occurs for the areas in and around Germany during the morning hours. Table 54 shows the percentage of times the cloud ceiling is less than l km for these regions. Note the relatively high percentage of time that a low cloud ceiling occurs throughout this area, especially in the winter.

**The former Czechoslovakia has been divided into the Czech Republic, which borders Germany, and Slovakia.*

†Not shown is the southern tip of Germany, which is contained within the Alpine region of the climatology database.

Figure 12. Regions from climatology database that contain German Lowlands (A), German Highlands (B), and Rhine Valley (C).

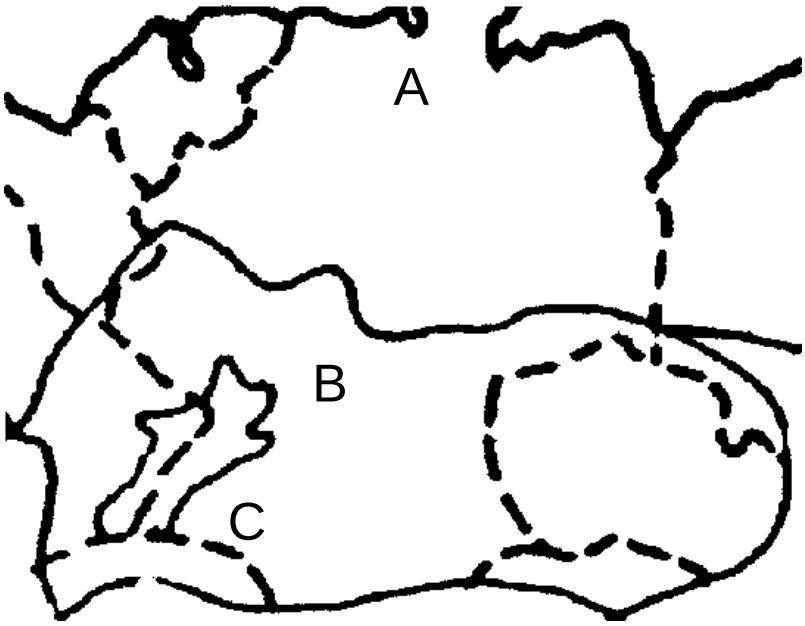

Table 41. Percentage of times fog with mean visibility ≤ 2 km occurs in Lowlands.

Time of day	Winter	Spring	Summer	Autumn
0300–0900	16.7	12.6	11.8	23.9
1000–1400	17.0	5.0	1.8	10.7
1500–1900	13.2	2.2	0.4	5.7
2000–0200	14.6	5.6	3.2	12.7

Table 42. Percentage of times fog with mean visibility < ~0.5 km occurs in Lowlands.

Time of day	Winter	Spring	Summer	Autumn
0300–0900	6.4	4.4	3.7	11.1
1000–1400	5.5	1.1	0.2	3.2
1500–1900	3.6	0.3	0.0	1.1
2000–0200	5.0	1.3	0.6	4.8

Table 43. Percentage of times cloud ceiling < 1 km occurs in Lowlands.

Time of day	Winter	Spring	Summer	Autumn
0300–0900	54.3	35.6	26.2	34.6
1000–1400	54.4	42.3	32.5	38.2
1500–1900	50.2	30.3	19.8	26.5
2000–0200	50.0	26.2	16.4	24.8

Table 44. Percentage of times cloud ceiling < 1 km minus percentage of times rain with visibility < 1 km occurs in Lowlands.

Time of day	Winter	Spring	Summer	Autumn
0300–0900	53.4	35.1	25.9	34.1
1000–1400	53.3	42.0	32.4	27.9
1500–1900	49.3	30.1	19.8	26.3
2000–0200	49.3	26.0	16.3	24.6

Table 45. Percentage of times fog with mean visibility ≤ 2 km occurs in Highlands.

Time of day	Winter	Spring	Summer	Autumn
0300–0900	17.4	9.0	9.7	24.5
1000–1400	15.3	3.2	1.6	9.8
1500–1900	11.2	1.6	0.9	4.3
2000–0200	14.4	2.3	2.9	12.0

Table 46. Percentage of times fog with visibility < ~300 m occurs in Highlands.

Time of day	Winter	Spring	Summer	Autumn
0300–0900	9.5	4.1	9.7	14.9
1000–1400	6.7	1.2	1.6	4.4
1500–1900	4.9	0.8	0.9	1.9
2000–0200	7.5	1.8	2.9	6.4

Table 47. Percentage of times cloud ceiling < 1 km occurs in Highlands.

Time of day	Winter	Spring	Summer	Autumn
0300–0900	60.6	36.7	27.1	41.6
1000–1400	59.1	43.2	33.6	42.3
1500–1900	53.8	32.3	22.4	29.0
2000–0200	55.3	28.5	18.9	29.8

Table 48. Percentage of times cloud ceiling < 1 km minus percentage of times rain with visibility < 1 km occurs in Highlands.

Time of day	Winter	Spring	Summer	Autumn
0300–0900	59.4	35.1	26.4	40.7
1000–1400	57.8	42.7	33.0	41.6
1500–1900	52.9	31.9	21.9	28.4
2000–0200	54.2	28.1	18.4	29.1

Table 49. Percentage of times fog with mean visibility ≤ 2 km occurs in Rhine Valley.

Time of day	Winter	Spring	Summer	Autumn
0300–0900	15.7	6.2	7.4	24.1
1000-1400	17.3	2.9	1.3	12.0
1500–1900	12.1	0.7	0.3	5.7
2000–0200	14.0	0.3	1.3	12.2

Table 50. Percentage of times fog with mean visibility < ~0.5 km occurs in Rhine Valley.

Time of day	Winter	Spring	Summer	Autumn
0300–0900	6.7	1.5	1.8	12.4
1000–1400	5.4	0.3	0.0	4.0
1500–1900	3.7	0.0	0.0	1.0
2000–0200	5.3	0.3	0.2	5.3

Table 51. Percentage of times cloud ceiling < 1 km occurs in Rhine Valley.

Time of day	Winter	Spring	Summer	Autumn
0300–0900	45.3	20.3	13.3	30.4
1000-1400	44.3	24.0	15.9	28.3
1500-1900	38.5	14.8	7.6	15.3
2000-0200	40.0	13.4	7.3	17.6

Table 52. Percentage of times cloud ceiling < 1 km minus percentage of times rain with visibility < 1 km occurs in Rhine Valley.

Time of day	Winter	Spring	Summer	Autumn
0300–0900	44.8	20.2	13.3	29.9
1000–1400	43.8	23.9	15.9	28.0
1500–1900	38.0	14.8	7.6	15.2
2000–0200	39.6	13.4	7.3	17.4

Table 53. Percentage of times fog with mean visibility ≤ 2 km occurs for regions in and around Germany.

Winter	Spring	Summer	Autumn
17	9	10	24

Table 54. Percentage of times cloud ceiling < 1 km occurs for regions in and around Germany.

Regions	Winter	Spring	Summer	Autumn
European Highlands	57	35	26	46
European Lowlands	52	34	24	31
Rhine Valley	42	18	11	25

3.4 Mideast

There probably is no universally accepted definition of the Mideast area. The Encyclopedia Britannica defines the Mideast as the lands around the southern and eastern shores of the Mediterranean Sea, extending from Morocco to the Arabian Peninsula and Iran and sometimes beyond. The climatology database considers the Persian Gulf and the stripped area shown in figure 13, which is called the Mideast Desert, to be the Mideast [8].

3.4.1 Mideast Desert

Tables 55 through 57 show fog and cloud information for the Mideast Desert region.

3.4.2 Persian Gulf

Tables 58 through 60 show fog and cloud information for the Persian Gulf region.

3.4.3 Summary

In the Mideast (the Mideast Desert and the Persian Gulf) there is a low percentage of times that fog occurs. The worst occurrence of fog is 4 percent of the time during the morning hours during the winter and autumn in the Persian Gulf, and during the winter in the Mideast Desert. Even though the skies are generally considered to be clear throughout the year, during the winter a cloud ceiling less than 1 km occurs 19 percent of the time in the Mideast Desert and 9 percent of the time in the Persian Gulf.

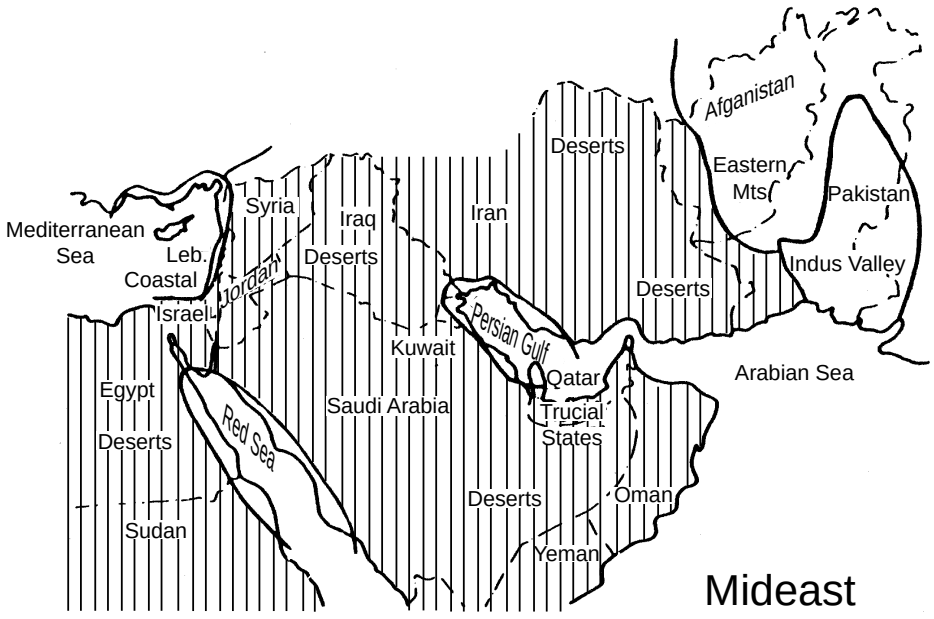

Figure 13. Regions from climatology database that contain Mideast. Striped area is Mideast Desert. Persian Gulf is in center of figure.

Table 55. Percentage of times fog with mean visibility ≤ 2 km occurs in Mideast Desert.

Time of day	Winter	Spring	Summer	Autumn
0300–0900	3.9	0.9	0.8	1.1
1000–1400	1.8	0.7	1.2	0.8
1500–1900	0.9	0.5	0.8	0.6
2000–0200	1.4	0.2	0.1	0.2

Table 56. Percentage of times cloud ceiling < 1 km occurs in Mideast Desert.

Time of day	Winter	Spring	Summer	Autumn
0300–0900	18.1	10.5	3.1	5.8
1000–1400	21.0	13.9	2.3	7.6
1500–1900	18.3	13.4	1.7	5.7
2000–0200	16.7	9.7	2.3	5.6

Table 57. Percentage of times cloud ceiling < 1 km minus percentage of times rain with visibility < 1 km occurs in Mideast Desert.

Time of day	Winter	Spring	Summer	Autumn
0300–0900	18.0	10.4	3.0	5.7
1000–1400	20.9	13.8	2.2	7.5
1500–1900	18.2	13.3	1.6	5.6
2000–0200	16.6	9.6	2.2	5.5

Table 58. Percentage of times fog with mean visibility ≤ 2 km occurs in Persian Gulf.

Time of day	Winter	Spring	Summer	Autumn
0300–0900	3.5	0.8	0.5	3.5
1000–1400	1.8	0.2	0.2	0.6
1500–1900	0.4	0.0	0.0	0.1
2000–0200	0.9	0.2	0.1	0.7

Table 59. Percentage of times cloud ceiling < 1 km occurs in Persian Gulf.

Time of day	Winter	Spring	Summer	Autumn
0300–0900	8.9	4.8	0.9	3.3
1000–1400	12.0	5.9	1.4	2.8
1500–1900	10.4	5.8	2.1	2.1
2000–0200	6.6	3.9	1.0	1.5

Table 60. Percentage of times cloud ceiling < 1 km minus percentage of times rain with visibility < 1 km occurs in Persian Gulf.

Time of day	Winter	Spring	Summer	Autumn
0300–0900	8.8	4.7	0.9	3.2
1000–1400	11.9	5.9	1.3	2.7
1500–1900	10.3	5.7	2.1	2.0
2000–0200	6.6	3.8	0.9	1.4

4. Summary and Conclusions

Because the resolution of passive imaging systems varies as the wavelength divided by the aperture diameter, for practical aperture diameters there are more pixels on a target for an IR system than a MMW system. Under good weather conditions, this allows an IR radiometer to have a greater detectability range and better imaging qualities. However, under sufficiently adverse weather conditions an IR system cannot detect a target, while a MMW radiometer still might be able to detect that target.

This report examined passive IR system (FLIR) and passive MMW system performance through clouds, rain, fog, and, to a lesser extent, snow. NVESD's Acquire model was used to analyze the performance of FLIRs in rain and in not very dense fog. Because the Acquire model does not work for propagation media that have very low IR transmittance, such as clouds and dense fog, another method was needed to analyze FLIR performance in that medium. An assumption was made that a FLIR could not detect a target with 50-percent probability or better at a distance that corresponds to a transmittance of 0.01 or less. For passive MMW systems, the performance in adverse weather conditions was based on Wikner's report [3]. We determined that for propagation

- through widespread rain and drizzle, FLIRs outperform passive MMW systems;
- through thunderstorms neither FLIRs nor MMW systems work well; and
- through clouds and dense fog, passive MMW systems outperformed FLIRs.

A summary of the weather conditions that result in an advantage of passive MMW systems over passive IR systems is shown in table 61.

We did not address the gray area of when a MMW radiometer system just starts to outperform a FLIR; rather we addressed those conditions when a FLIR cannot detect an object and considered whether under those same conditions it is possible to detect an object with a MMW radiometer. Using the condition that the atmospheric transmittance equals 0.01 to determine the distance at which a FLIR fails to detect an object alleviates the need to compensate for the fact that different detection schemes are used for the MMW and the IR.

Table 61. Summary of advantages of passive MMW systems over passive IR systems.

Condition	Result
Rain	No advantage
Advective fog	Large advantage
Radiation fog	Large advantage over the 3- to 5-μm band
	Advantage over the 8- to 12-μm band when visibility ≤ 0.5 km
Clouds	Large advantage
Snow	Advantage

A similar analysis was used to show that passive MMW systems can outperform FLIRs in snow. However, the limitations in ARL's EOSAEL 92 Climatology Module make it impossible to determine from the climatology database the frequency of the occurrence of only snow for regions around the world, because the classes in the module are not mutually exclusive. For example, if the climatology database shows that snow occurs with visibility of 500 m, it is impossible to determine from the database if this is due to only snow or due to a combination of snow and fog.

Because the most significant advantage of MMW over FLIRs is through fogs and clouds, selected regions of the world were examined for the frequency of occurrence of cloud ceilings less than 1 km and fog with visibility less than 1 or 2 km. The weather statistics were taken from ARL's EOSAEL 92 Climatology Module. The regions were picked primarily because of potential military interest and secondly because of the high percentage of adverse conditions. The Adriatic Alps region (the area around the Adriatic Sea), which has good weather year round, was included because of its proximity to Bosnia and the fact that the nearby regions of the Balkan Highlands and Balkan Plains were examined.

Section 3 gives the percentage of times that the cloud ceiling is less than 1 km for selected locations around the world during the morning, midday, evening, and night for each of the four seasons. Because the variation in cloud coverage was generally not large during the day, the results were averaged throughout the day. Table 62 presents a summary of those results. The percentage of times that low cloud cover occurs is relatively high and is over 50 percent in some of the regions.

Selected fog information from section 3 is in tables 63 through 67. Table 63 gives a summary of the percentage of times that fog with mean visibility less than 2 km occurs for the regions in and around Bosnia, with the results averaged throughout the day. Note the high percentages in the winter. Also shown are the weather statistics for the Dinaric Alps from 0300-0900 during the autumn and winter (table 64), and weather statistics for the Balkan Highlands averaged over the time period 0300-1400 during the autumn and winter (table 65). Special emphasis is given to these regions because of the prominence of adverse weather and the military interest. Table 66 gives a summary of the percentage of times that fog with mean visibility less than 2 km occurs for the regions in and around Germany from 0300–0900. Note the high levels in the autumn. For the time periods after 0900, fog is not as prevalent in these regions except during the winter. During the winter, fog is prevalent throughout the day. This is shown in table 67, which summarizes the percentage of times that fog with mean visibility less than 2 km occurs for these regions, with the results averaged throughout the day.

The results in the EOSAEL's climatology database are averaged over a large area. In certain localities the frequency of occurrence of fog can be significantly higher. For instance, at the Wasserkuppe, Germany, weather station in December during the morning hours (0600, 0700, and 0800), the frequency of the occurrence of fog with visibility less than or equal to 0.5 km is 60 percent [9].

Table 62. Percentage of times cloud ceiling < 1 km occurs for selected locations.

Regions	Winter	Spring	Summer	Autumn
Korea East Coast	23	29	56	31
South Korea	24	27	40	24
West Korea	24	23	39	22
Dinaric Alps	41	27	23	34
Balkan Highlands	34	28	24	27
Balkan Plains	37	21	12	29
Adriatic Alps	13	9	3	10
European Highlands	57	35	26	46
European Lowlands	52	34	24	31
Rhine Valley	42	18	11	25
Persian Gulf	9	5	1	2
Mideast Desert	19	12	2	6

Table 63. Percentage of times fog with mean visibility < 2 km occurs for regions in and around Bosnia.

Regions	Winter	Spring	Summer	Autumn
Dinaric Alps	19	6	7	14
Balkan Highlands	18	12	12	14
Balkan Plains	18	3	1	10

Table 64. Weather statistics for Dinaric Alps from 0300–0900 during autumn and winter.

	Percentage of occurrence	
Condition	Autumn	Winter
Cloud ceiling ≤ 1 km	42	46
Fog with visibility ≤ 1 km	18	13
Fog with mean visibility ≤ 2 km	25	23
Snow with visibility ≤ 1 km	1	2
Snow with mean visibility ≤ 2 km	2	6

Table 65. Weather statistics for Balkan Highlands from 0300–1400 during autumn and winter.

	Percentage of occurrence	
Condition	Autumn	Winter
Cloud ceiling ≤ 1 km	28	35
Fog with mean visibility ≤ 200 m	13	15
Fog with mean visibility ≤ 2 km	15	20
Snow with visibility ≤ 1 km	2	6
Snow with mean visibility ≤ 2 km	3	8

Table 66. Percentage of times fog with mean visibility < 2 km occurs for regions in and around Germany (0300–0900).

Regions	Winter	Spring	Summer	Autumn
European Lowlands	17	13	12	24
European Highlands	17	9	10	25
Rhine Valley	16	6	7	24

Table 67. Percentage of times fog with mean visibility < 2 km occurs, averaged throughout day during winter for regions in and around Germany.

Regions	Percentage of occurrence
European Lowlands	15
European Highlands	15
Rhine Valley	15

Weather conditions that prevent FLIRs from detecting targets, but do not degrade MMW performance enough to prevent detecting those targets, occur a significant percentage of the time. The weather statistics indicate that the cloud height is less than 1 km in the selected regions about 25 percent of the time, and as high as 54 to 59 percent of the time in the Korean East Coast region during summer. Even in the Mideast Desert, this condition occurs 17 to 20 percent of the time during the winter. Indeed, the significance of the effects of clouds in the Mideast was evidenced by newspaper reports in September 1995 that mentioned that North Atlantic Treaty Organization (NATO) air strikes over Bosnia had to be canceled because of cloud coverage. Fog with visibility less than 2 km occurs about 20 percent of the time for winter mornings around Bosnia and 10 percent of the time for summer mornings in Korea.

References

1. J. Johnson, *Analysis of Image Forming Systems*, Proc. of Image Intensifier Symposium (October 1958).

2. Robert E. Roberts and Lynne N. Seekamp, *Infrared Attenuation by Aerosols in Limited Atmospheric Visibility: Relationship to Liquid Water Content*, Institute for Defense Analyses, Science and Technology Division, Arlington, VA (1979).

3. D. Wikner, *Prediction of 94 GHz Radiometer Performance in Various Environmental Condition for Army Applications*, Army Research Laboratory, ARL-TR-1103 (September 1996).

4. J. Nemarich, et al., *Comparative Near-Millimeter Wave Propagation Properties of Snow or Rain*, Proc. Snow Symposium III, U.S. Army Cold Regions Research and Engineering Laboratory, Hanover, NH (August 1983).

5. P. Bhartia, and I. J. Bahl, *Millimeter Wave Engineering and Applications*, John Wiley and Sons, Inc., New York (1984).

6. Bruce T. Miers, Elton P. Avara, and Louis D. Duncan, *Global Electro-Optical Systems Environmental Matrix (GEOSEM) Climatology for Korea*, ASL-TR-175, U.S. Army Electronics Research and Development Command, Atmospheric Sciences Laboratory, White Sands Missile Range, NM (1985).

7. Bruce T. Miers, Elton P. Avara, and Louis D. Duncan, *Global Electro-Optical Systems Environmental Matrix (GEOSEM) Climatology for the Northern Mediterranean Area and Southern Europe*, ASL-TR-201, U.S. Army Laboratory Command, Atmospheric Sciences Laboratory, White Sands Missile Range, NM (1986).

8. Bruce T. Miers, Elton P. Avara, and Louis D. Duncan, *Global Electro-Optical Systems Environmental Matrix (GEOSEM) Climatology for Mideast and Southwest Asia*, ASL-TR-172, U.S. Army Electronics Research and Development Command, Atmospherics Sciences Laboratory, White Sands Missile Range, NM (1985).

9. Robert G. Humphrey and William H. Pepper, *Environmental Standards for Electro-Optical Systems*, Harry Diamond Laboratories, HDL-TR-2007 (April 1983).

Appendix. IR and MMW Imager Theory

This appendix examines the basic detection schemes of MMW imagers and the Army's most common type of passive IR imager, forward-looking infrared (FLIR). For MMW imagers, a metal target's signature is determined with the use of reflected natural radiation, because such a target has a low emissivity and high reflectivity at MMW frequencies. Background objects usually have high emissivities, and the ability of the imager to detect the target is based on the temperature difference between the relatively cold sky temperature reflected by the target and the background temperature. This temperature difference can be as large as 100 K. FLIRs measure the apparent temperature difference between the target's and the background's temperature, both of which may have relatively high emissivity. If we assume that the temperature of the target and the background are approximately the same, as is true, for example, for a parked vehicle at night with an engine that has not been running for several hours, then the dominant IR target signature is primarily due to the difference in the target's and the background's emissivity* and is about 1 K. However, if the sensor is looking at a hot source, for example, a running engine or its exhaust, or a surface heated by the sun, then the temperature difference between the background and the object can be much greater.

A-1 Passive Detection

Passive systems rely on the thermal radiation of a target as a means to detect and image the target, while active systems rely on a transmitted beam to scatter the energy off a target as a means to detect and image it. Some of the advantages of passive systems over active systems are that they

(1) have a signal that is proportional to r^{-2} as opposed to r^{-4}, where r is the distance between the sensor and the object;

(2) have a sensor that is more difficult to detect;

(3) have better imaging characteristics;† and

(4) are smaller and lighter.

A-1.1 MMW Radiometers

When radiation is incident on an object, some of it is reflected by the object and the rest penetrates into the object. The radiation that penetrates into the object is either absorbed and converted into internal energy or is transmitted through the material. An object that absorbs all the incident

**In general, this is not true. If the sensor is looking at a hot source (for example, a running engine or its exhaust, or a surface heated by the sun), then the temperature difference between the background and the object can be large.*

†Usually, radiation is not scattered in all directions (diffuse reflection) but is scattered more strongly in one or more directions (specular reflections). These specular reflections give images with degraded quality to the active systems.

radiation and converts it into internal energy (i.e., no reflected or transmitted radiation) is a blackbody. By absorbing the maximum radiation at all wavelengths, a blackbody, as a consequence of the second law of thermodynamics, emits the maximum amount of radiation.

Planck's radiation law gives the radiation of a blackbody in terms of its brightness (B) by

$$B = \frac{2h\nu^3}{c^2} \frac{1}{e^{h\nu/kT} - 1} \ , \tag{A-1}$$

where h = Planck's constant,

ν = the frequency of the radiation,

c = the speed of light,

k = Boltzmann's constant, and

T = temperature.

The equation also gives a measurement of the power received per unit area per unit solid angle per unit bandwidth ($Wm^{-2}\ sr^{-1}\ Hz^{-1}$).*

For millimeter waves, the wavelength $\lambda \approx 1$ mm or greater; at room temperature $kT = 0.025$ eV, therefore,

$$\frac{hc}{\lambda kT} \leq 0.08 \ . \tag{A-2}$$

Because this is much less than 1,

$$e^{hc/\lambda kT} \approx 1 + \frac{hc}{\lambda kT} \ . \tag{A-3}$$

Inserting equation (A-3) into equation (A-1) and using the relationship $c = \lambda\nu$, yields

$$B \approx \frac{2k}{\lambda^2} T \ . \tag{A-4}$$

**If we multiply both sides of equation (A-1) by dv and note that $dv = -c\, d\lambda/\lambda^2$, we can express the brightness in terms of unit wavelength by*

$$B_\lambda = \frac{2hc^2}{\lambda^5} \frac{1}{e^{hc/kT\lambda} - 1} \ .$$

This is called the spectral radiance L and is a measurement of the power received per unit area per unit solid angle per unit wavelength ($W\ cm^{-2}\ sr^{-1}\ \mu m^{-1}$). Many textbooks give Planck's radiation law in terms of the spectral existence M, where $M = \int_{hemisphere} d\Omega L(\phi,\theta)$. For a Lambertian surface this equals $L\int_0^{2\pi}\int_0^{\pi/2} \cos\theta\, d\Omega = \pi L$. Because a blackbody (bb) is a Lambertian surface we have that $M_{bb} = \frac{2\pi hc^2}{\lambda^5} \frac{1}{e^{hc/kT\lambda} - 1}$ ($W\ cm^{-2}\ sr^{-1}\ \mu m^{-1}$), which is probably the most common expression of Planck's radiation law.

Hence the thermal source brightness, which is proportional to the power emitted by a blackbody source at millimeter wavelengths, varies with the temperature.

Because no object is a perfect blackbody,* the amount of radiation an object emits is less than that of a blackbody by a factor of $\varepsilon(\lambda)$, called the emissivity. Consequently, the thermal radiation emitted by an object is proportional to the product $\varepsilon(\lambda)\, T$. This proportionality allows the radiation emitted by the object to be expressed in terms of temperature.

The remainder of section A-1.1 is taken primarily from W. J. Wilson, et al [A-1].

When an MMW sensor is looking down on an object, its total received radiation is due to the object emissions, the sky emissions that the object reflects, the background emissions that are also in the antenna's beam area, and the emissions from the atmosphere between the radiometer and the object. Summarizing, the total received radiation in terms of measured brightness temperature is given by

$$T_{\text{total}} = T_{\text{object}} + T_{\text{reflected sky}} + T_{\text{background}} + T_{\text{atmosphere}} . \qquad \text{(A-5)}$$

If the object does not fill the field of view of the MMW sensor, a fill factor η has to be considered, where η is the ratio of the object's area to the antenna's main beam area. Because the thermal radiation of the object is attenuated by the atmosphere, the received radiation in the measured brightness temperature is reduced by an atmospheric attenuation factor L_a, where L_a is defined as

$$L_a = 10^{(L_{atm}\, R / 10^4)} , \qquad \text{(A-6)}$$

where L_{atm} is the attenuation between the sensor and the object in decibels per kilometer, and R is the distance between the sensor and the object in meters.

Using the above definitions, the measured brightness temperature from the object is given as

$$T_{\text{object}} = \frac{\varepsilon T \eta}{L_a} . \qquad \text{(A-7)}$$

The sky temperature results from atmospheric emission and varies with meteorological conditions and the zenith angle θ (see figs. A-1 and A-2). At the zenith angle θ, the sky temperature is given by†

$$T_{\text{sky}} = \sec\theta \int_0^\infty \alpha(z)\, T(z) \exp\left(- \int_0^z \alpha(z') \sec\theta \, dz' \right) dz , \qquad \text{(A-8)}$$

where α is the attenuation coefficient of the atmosphere per unit length, and T is the brightness temperature of the stratum at a height z and vertical thickness dz.

**Some surfaces such as carbon black, carborundum, platinum black, and gold black come close.*

†Equation (A-8) is valid as long as the sun does not enter the beam that goes from the sensor to the object. See Bhartia and Bahl [A-2].

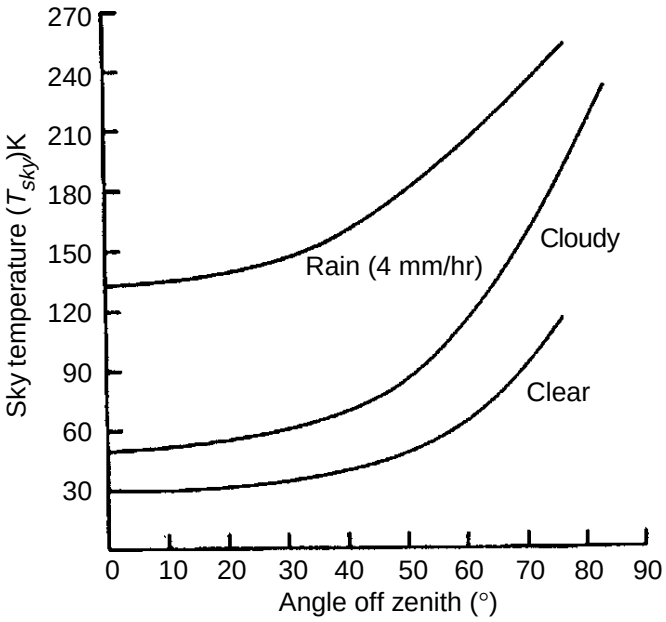

Figure A-1. Radiometric sky temperature at 35 GHz under different environmental conditions.

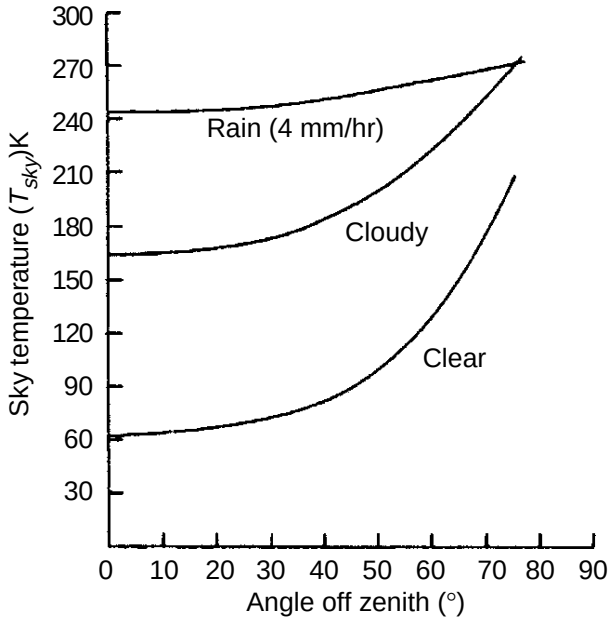

Figure A-2. Radiometric sky temperature at 95 GHz under different environmental conditions.

The amount of energy that is reflected by the object and incident on the sensor is proportional to the fill factor η, and the reflection coefficient $\rho = 1 - \varepsilon$,* and is reduced by the atmospheric absorption factor L_a. This gives the expression for the reflected sky temperature as

$$T_{\text{reflected sky}} = \frac{(1-\varepsilon)T_{sky}\eta}{L_a} \quad . \tag{A-9}$$

If the object does not fill the field of view of the MMW sensor, then the antenna will see the background. This background, which has an emissivity

**This assumes that no energy is transmitted through the object.*

ε_g, reflectivity $(1 - \varepsilon_g)$, and temperature T_g, will emit thermal radiation and reflect the sky radiation. Thus,

$$T_{\text{background}} = \left(\frac{\varepsilon_g T_g + \left(1 - \varepsilon_g\right) T_{sky}}{L_a} \right) (1 - \eta) \ . \tag{A-10}$$

Radiation that propagates through the atmosphere is attenuated by absorption and emitted as thermal energy. The brightness (or apparent) temperature from the emissions of the atmosphere that is contained in the path from the sensor to the object is expressed as

$$T_{atm} = T_a \left(1 - \frac{1}{L_a} \right) , \tag{A-11}$$

where T_a is the actual temperature of the atmosphere below the MMW sensor. If there is no atmospheric absorption (i.e., attenuation) then L_{atm} equals 0,which implies L_a equals 1, which implies T_{atm} equals 0.

Inserting equations (A-7), (A-9), (A-10), and (A-11) into equation (A-5) gives the expression for the total received temperature as

$$\begin{aligned} T_{\text{total}} = & \frac{\varepsilon T \eta}{L_a} + \frac{(1 - \varepsilon) T_{\text{sky}} \eta}{L_a} \\ & + \left(\frac{\varepsilon_g T_g + \left(1 - \varepsilon_g\right) T_{\text{sky}}}{L_a} \right) (1 - \eta) + T_a \left(1 - \frac{1}{L_a} \right) . \end{aligned} \tag{A-12}$$

Equation (A-12) can be used to calculate the temperature contrast between scenes with and without a target. As an example, consider a metal target that comes into the field of view of the sensor. Assume the emissivity of the metal equals 0, and the emissivity of the background equals 1. Then before the target enters the scene,

$$T_{\text{total}} = \frac{T_g}{L_a} + T_a \left(1 - \frac{1}{L_a} \right) . \tag{A-13}$$

When the target enters the scene, we obtain

$$T_{\text{total}} = \frac{T_{\text{sky}} \eta}{L_a} + \frac{T_g}{L_a} (1 - \eta) + T_a \left(1 - \frac{1}{L_a} \right) . \tag{A-14}$$

The contrast temperature is obtained by subtracting equation (A-14) from equation (A-13), or

$$\Delta T = \frac{\eta}{L_a} \left(T_g - T_{\text{sky}} \right) . \tag{A-15}$$

Table A-1 shows the calculated temperature contrasts for clear, cloudy, and rainy conditions. Assumed values of a 10-percent fill factor ($\eta = 0.1$) and a background temperature of 300 K were used in equation (A-15).

A-1.2 FLIR Imagers

This section briefly explains the process by which an acquisition task, such as detection or recognition, is performed with a FLIR imager. FLIRs collect and image IR photons from an object analogous to how video cameras collect and image visible photons from an object. They operate in two IR bands, the 3- to 5-μm or medium-wave infrared (MWIR) band and the 8- to 12-μm or long-wave infrared (LWIR) band. Both bands have advantages and disadvantages. For example, the MWIR band is able to detect exhaust gas emission better than the LWIR band, but is more susceptible to sun glint and fog.

The figure of merit that will be used to evaluate FLIR performance is the minimum resolvable temperature (difference) or MRT. MRT is the best overall indicator of thermal imager performance according to NVESD's FLIR92 Thermal Imagery Systems Performance Model. MRT is related to the minimum temperature difference required to distinguish a target from its background. More precisely, MRT is a measure of the observer's ability to distinguish between bar targets and the space between them. It is defined as "the minimum temperature difference above 300 K required by an observer to resolve a vertical four bar pattern of a 7:1 aspect ratio"[A-3]. Clearly, MRT is a function of the spatial frequency of the image, which in turn depends on the size of and range to the target. The advantage of MRT over other system parameters, such as noise equivalent temperature (NET), is that it is indicative of overall system performance, including the observer. The MRT incorporates various system parameters such as NET, modulation transfer function (MTF), signal-to-noise threshold (SNRT), and noise filter factor ρ_x. I will discuss each of these system parameters and explain the spatial frequencies. At the end of this appendix, I also discuss another overall performance indicator, the minimum detectable temperature difference or MDT, which is used for pure detection.

Spatial frequency.—Whereas temporal frequency is a variation of the amplitude of the signal with respect to time or cycles per second, spatial frequency is a variation of the amplitude of the signal with respect to space or cycles per meter. Figure A-3, shows four cycles per meter on a target, where a cycle is a 7:1 aspect ratio bar and a 7:1 aspect ratio space, or one line pair.

Table A-1. Temperature contrasts for various conditions.

Condition	T_{sky}	L_a	ΔT
Clear	65	1.15	20
Cloudy	175	3	4.2
Rain (4 mm / hr)	245	1.2	0.5

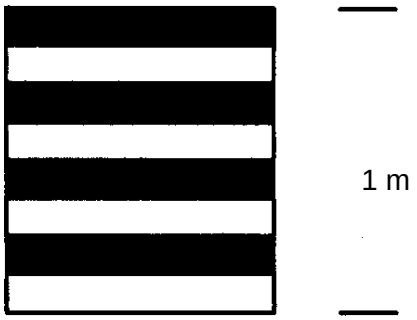

Figure A-3. Four cycles per meter shown on target.

For FLIRs, it is more convenient to convert the linear spatial frequency of cycles per meter to an angular spatial frequency v in terms of cycles per milliradians, where

$$v = \frac{R\,N}{1000\,D} \ , \qquad \text{(A-16)}$$

and

D = a representative dimension,
N = the number of bar pairs across D, and
R = the distance from the FLIR to the object.

The advantage of using angular spatial frequency is that in the focal plane of a FLIR the angular spatial frequency is the same as in the object space. As shown in figure A-4, the instantaneous field of view of a detector is the same as the detector's angular subtense; this allows the FLIR's pixel size to be related to the number of cycles on the target.

In figure A-4,

f = the detector focal length,
Δx = the in-scan detector subtense,
Δy = the cross-scan detector subtense,
a = the in-scan detector dimension,
b = the cross-scan detector dimension, and
R = the distance from the FLIR to the object.

Johnson criteria.—Johnson [A-4] related the ability of an observer to resolve a number of line pairs across the minimum dimension of selected military targets to the ability of the observer to perform the tasks of detection, orientation, recognition, and identification with 50 percent probability. This is illustrated in figure A-5; the results were derived through an extensive series of measurements. For example, according to figure A-5, an observer using a FLIR has to be able to discern 3.5 bar pairs across the minimum dimension of an M-48 tank to recognize it.

When Johnson performed his experiments in the late 1950s to determine a person's ability to perform certain acquisition tasks with 50 percent probability, he used the minimum dimension of the target as the size parameter. A better parameter is the critical dimension,

$$D_c = \sqrt{lh\cos\theta\sin\phi + wh\cos\phi\sin\phi + lw\sin\theta\cos\theta} \ . \qquad \text{(A-17)}$$

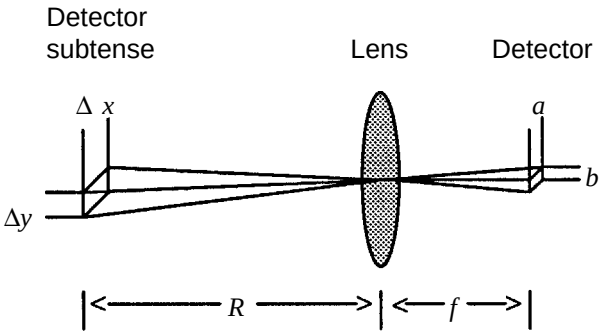

Figure A-4. Relationship between detector subtense and instantaneous field of view.

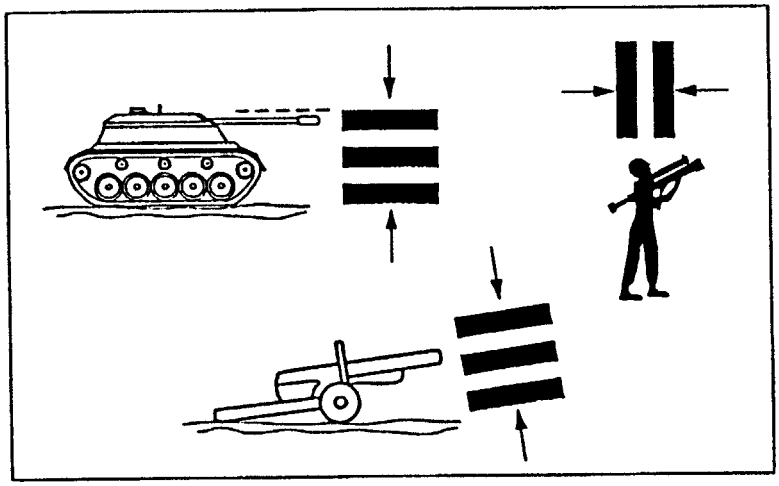

Figure A-5. Resolution required for acquisition tasks of detection, orientation, recognition, and identification based on Johnson criteria [A-4].

Broadside view	Detection	Orientation	Recognition	Identification
Truck	0.90	1.25	4.5	8.0
M-48 tank	0.75	1.2	3.5	7.0
Stalin tank	0.75	1.2	3.3	6.0
Centurion tank	0.75	1.2	3.5	6.0
Half-track		1.5	4.0	5.0
Jeep	1.2	1.5	4.5	5.5
Command car	1.2	1.5	4.3	5.5
Soldier	1.5	1.8	3.8	8.0
105-mm howitzer	1.0	1.5	4.8	6.0
Average	1.0 ± 0.24	1.4 ± 0.35	4.0 ± 0.8	6.4 ± 1.5

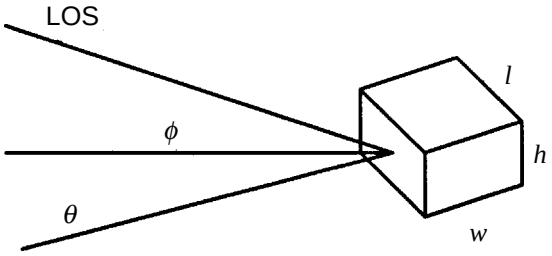

Figure A-6. Orientation of equivalent parallelepiped of target with respect to line of sight.

As shown in figure A-6, the parameters *l*, *w*, and *h* are the unobstructed dimensions of an equivalent parallelepiped; ϕ is the azimuth angle; and θ is the elevation angle, which is the angle between the line of sight from the observer to the target and the ground. If part of the target is obstructed, that part is not used to compute the critical dimension.

I now discuss the system parameters that are incorporated into MRT.

NET.—Historically, NET has been used as a performance indicator of noise characteristics or sensitivity of IR detectors. NET is the required temperature difference between an object and its background that will produce a signal-to-noise ratio of unity. An expression for NET [A-5] is

$$\mathrm{NET} = \frac{0.04\, F^2 \Delta F^{1/2}}{\pi A_D^{1/2}\, \tau_0\, D^*\, H}\ (\mathrm{K})\ , \tag{A-18}$$

where

F = the system focal ratio or F number,
ΔF = the noise equivalent bandwidth in hertz,
A_D = the area of the detector in square meters,
τ_0 = the optics transmission,
D^* = the band average detectivity in $\mathrm{Hz}^{1/2} \bullet \mathrm{W}^{-1}$, and
H = a value that expresses the amount of power being radiated by a blackbody source per unit area per steradian per Kelvin and is related to the temperature derivative of Plank's radiation at 300 K. It is equal to 6.3×10^{-5} W • cm^{-2} • K^{-1} • sr^{-1} for the 8- to 12-μm band and 6.7×10^{-6} W • cm^{-2} • K^{-1} • sr^{-1} for the 3- to 5-μm band.

MTF.—In scalar linear system theory applied to signals varying temporally, a system is characterized by a transfer function, $h(f)$, which gives the ratio of the output to the input for every frequency in a given band. For signals varying spatially, as in an imaging system, the analogy to $h(f)$ is the MTF. The MTF is the ratio of the output amplitude of an optical system to the input amplitude as a function of spatial frequency. The MTF of a FLIR is the product of several component MTFs, such as the electronics, preamplifier, eye, optical system, display, detector aperture, and detector temporal response MTF. Ratches [A-3] gives equations for several component MTFs and DCS Corporation [A-5] describes the component MTFs in detail. A representative MTF curve* is shown in figure A-7.

SNRT.—The spatial and temporal integration that the eye performs on the target has an effect on how the observer perceives the display. A factor called the perceived signal-to-noise ratio or SNRP takes this effect into account. The SNRT, that is the signal-to-noise threshold, is the experimentally determined SNRP characterizing a target, which is detected half the time. The probability of detection is a Gaussian distribution, evaluated at (SNRP– SNRT) and given by

**The MTF curve was created by doing a quadratic fit on some MTF values that were given by DCS Corporation [A-5].*

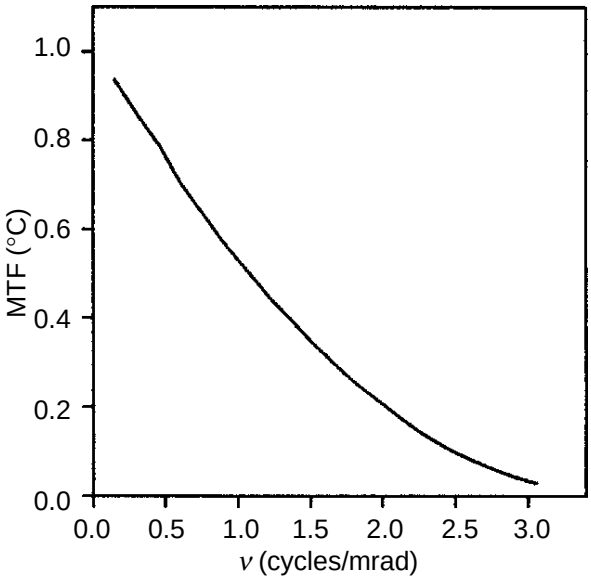

Figure A-7. MTF curve for representative system.

$$\text{probability of detection} = \frac{1}{\sqrt{2\pi}} \int_{-\infty}^{\text{SNRP–SNRT}} e^{-x^2/2} dx \ ; \qquad \text{(A-19)}$$

SNRT has an experimental value of 2 to 3.

Noise filter factor.—The noise filter factor ρ_x accounts for an improvement in the perceived SNRP due to some of the component MTFs that filter the noise as well as the signal.

MRT.—We can now express the minimum resolvable temperature as [A-5]

$$\text{MRT}(\nu) = \frac{2\text{SNRT NET}\rho_x^{1/2}}{\text{MTF}(\nu)} \left[\frac{\nu^2 \Delta x \, \Delta y}{L}\right]^{1/2} \left[t_e F_r\right]^{-1/2} , \qquad \text{(A-20)}$$

where

t_e = the eye integration time, which is around 0.1 to 0.2 s,
F_r = the frame rate, and
L = 7, which is the length-to-width ratio of the MRT bar.

Values from the MTF curve in figure A-7 and the values listed below [A-5] were inserted into equation (A-20) to create the MRT curve shown in figure A-8.

$$\text{SNRT} = 2.5$$
$$\rho_x = \frac{1}{\sqrt{1 + (0.67\nu)^2}} ,$$

Δx = 0.25 mrad,
Δy = 0.25 mrad,
t_e = 0.1 s,
F_r = 30 s^{-1}, and
NET = 0.1 K.

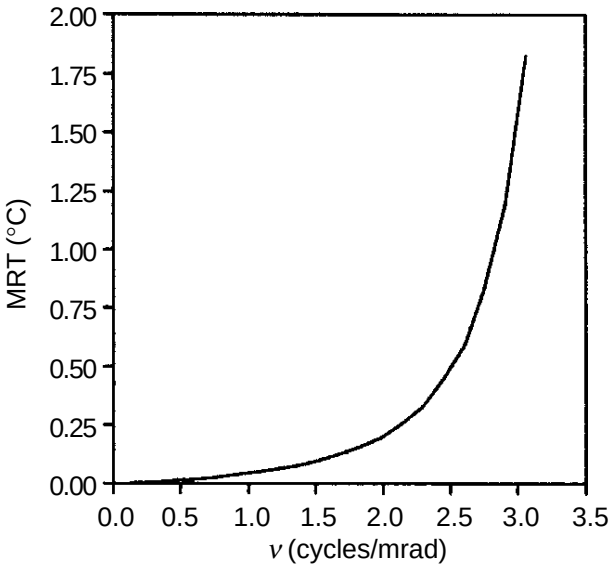

Figure A-8. MRT curve for representative system.

The MRT curve approaches an asymptote for $\nu = \frac{1}{\Delta x}$. This results from the limitation of the resolution of the detector.

Detection Range.—The following procedure, taken from *Infrared Imaging System Analysis* [A-5], shows how to calculate the distance at which a T-32 tank can be detected with an 8- to 12-μm FLIR under the following conditions:

1. Atmospheric transmittance = 0.6 at 1 km.

2. ΔT = 1 K.

3. Tank is at ground level, azimuth angle ϕ = 45°.

The detection distance is calculated by the intersection of two curves plotted as functions of range. The first curve is the product of ΔT, the temperature difference between the target and the background, and τ_a, the atmospheric transmittance; and shows how the apparent temperature decreased with range to the sensor due to atmospheric attenuation. The second curve plots the increase of MRT(ν) as a function of range; the ν dependence of MRT has been converted to range dependence by

$$\nu_i = \frac{R_i N_c}{1000 D_c} \ , \qquad \text{(A-21)}$$

which shows that ν is a function of the number of cycles N_c across the target as defined by the Johnson criteria, and the critical dimension D_c of the target, as well as range.

A maximum range R_m is chosen that will ensure that the two curves intersect. Instead of plotting graphs we can divide R_m into 15 to 20 equal parts and construct a table or worksheet.

One of the first steps in constructing the worksheet is to calculate the critical dimension of the T-32 tank. The equivalent parallelepiped dimensions are

l = 6.7 m,
w = 3.4 m, and
h = 2.4 m.

For this example the observer is taken to be at ground level, so the elevation angle is 0. The critical dimension of the tank is calculated from equation (A-17) to be 4.14 m. Because the elevation angle is 0, it does not change as the observer approaches the tank; therefore, the critical dimension is a constant.

For this example, assume that experience gives R_m to be 8000 m. Therefore, worksheet A-1 has R_m entries from 400 to 8000 in increments of 400 m. N_c is chosen to be the average for the three tanks listed in figure A-5, that is, N_c = 0.75. Using these values, the spatial frequencies v were calculated from equation (A-21) and the MRTs were obtained from figure A-8. The values were then inserted into worksheet A-1.

Worksheet A-1 shows that the two curves intersect at 6 km, yielding the distance at which the tank can be detected with 50-percent probability.*

One of the advantages of using MRT is that it can be used to calculate other acquisition tasks such as orientation, recognition, and identification. If the T-32 tank in the previous example is to be identified rather than just detected, then N_c = 6.3, obtained as the average of the three tanks in figure A-5. For this case, worksheet A-2 shows the information that is needed to compute the range at which a tank can be identified with 50-percent probability, which is 1600 m.

MDT.—For pure detection, the minimum detectable temperature, is probably a better criterion than MRT. Whereas MRT is a measure of the ability of an observer to resolve a certain number of bar targets across an object, MDT is a measure of the ability of an observer to detect a square. In contrast to the MRT curve, the MDT curve does not have an asymptote, because any object can be detected if it is hot enough.

Figure A-9 shows a comparison of MDT and MRT. If values from the MDT curve instead of the MRT curve and values from

$$v_i = \frac{R_i}{2000 D_c} \tag{A-22}$$

instead of equation (A-8), are used in the worksheet, then the procedure for determining the detection range using MDT is identical to the procedure using MRT.

**The critical dimension D_c can be adjusted so that this procedure will give a probability other than 50 percent to perform an acquisition task. For example, if D_c is changed from 4.14 to 2.31 m, then this procedure will give the distance at which the tank can be detected with 90-percent probability.*

Worksheet A-l. Values of R_m from 400 to 800 m.

Range (m)	D_c (m)	v (cy / mrad)	MRT (K)	$\Delta T \tau_a$ (K)
400	4.14	0.07	0.00	0.82
800	4.14	0.14	0.00	0.66
1200	4.14	0.22	0.01	0.54
1600	4.14	0.29	0.01	0.44
2000	4.14	0.36	0.01	0.36
2400	4.14	0.43	0.01	0.29
2800	4.14	0.51	0.02	0.24
3200	4.14	0.58	0.02	0.20
3600	4.14	0.65	0.02	0.16
4000	4.14	0.72	0.03	0.13
4400	4.14	0.80	0.03	0.11
4800	4.14	0.87	0.04	0.09
5200	4.14	0.94	0.04	0.07
5600	4.14	1.01	0.05	0.06
6000	4.14	1.09	0.05	0.05
6400	4.14	1.16	0.06	0.04
6800	4.14	1.23	0.07	0.03
7200	4.14	1.30	0.07	0.03
7600	4.14	1.38	0.08	0.02
8000	4.14	1.45	0.09	0.02

Worksheet A-2. Values of R_m from 100 to 2000 m.

Range (m)	D_c (m)	v (cy / mrad)	MRT (K)	$\Delta T \tau_a$ (K)
100	4.14	0.15	0.00	0.95
200	4.14	0.31	0.01	0.90
300	4.14	0.46	0.02	0.86
400	4.14	0.61	0.02	0.82
500	4.14	0.76	0.03	0.77
600	4.14	0.91	0.04	0.74
700	4.14	1.07	0.05	0.70
800	4.14	1.22	0.07	0.66
900	4.14	1.38	0.08	0.63
1000	4.14	1.53	0.10	0.60
1100	4.14	1.68	0.13	0.57
1200	4.14	1.83	0.16	0.54
1300	4.14	1.99	0.20	0.52
1400	4.14	2.14	0.26	0.49
1500	4.14	2.29	0.33	0.47
1600	4.14	2.44	0.44	0.44
1700	4.14	2.60	0.59	0.42
1800	4.14	2.75	0.83	0.40
1900	4.14	2.91	1.20	0.38
2000	4.14	3.06	1.83	0.36

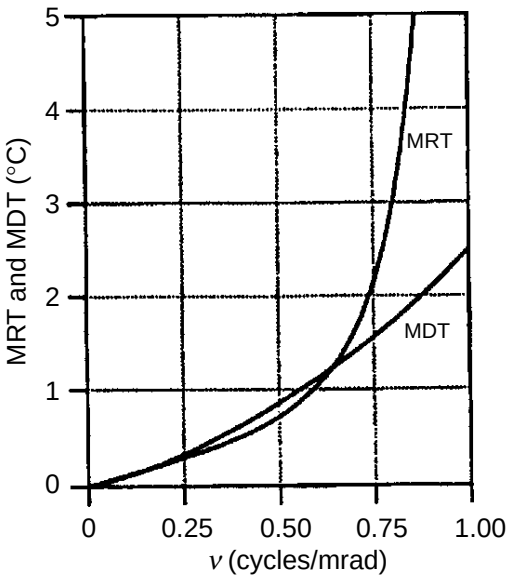

Figure A-9. Detector-limited MRT and MDT curves (taken from *Infrared Imaging System Analysis* [A-5], p 8-68).

A-1. 3 Diurnal Effects

Diurnal effects that produce "washout" in IR imagers became apparent during the Gulf War. During the day the target and the background heat up and cool down at different rates. They heat up during the daylight hours due to solar radiation and cool down during the night due to the heat reradiating into space. Because the heating and cooling rate of the target—for example, a tank—and the background are different, ΔT can go to 0 twice a day. During that time, that is, when $\Delta T\ \tau_a < 0.01$, the IR signal will experience washout.

Figure A-10 [A-5] shows the diurnal variation of ΔT, the temperature difference between a tank and the background, in central Europe under clear conditions. Figure A-11 [A-5] shows the same thing under cloudy conditions. Typically, twice a day ΔT goes to 0, resulting in a washout of the IR image.

Because MMW radiometers detect objects by the difference between the cold reflected sky temperature and the background (that is, they do not depend on the temperature of the target), they are not as affected by diurnal effects.

A-2 Atmospheric Effects

The propagation medium, or atmosphere, has a major impact on the performance of MMW and IR systems. The two major factors are the absorption of radiation by the molecules in the atmosphere and the scattering of radiation by particles such as water droplets.*

The atmosphere is made up of 15 gases. Nitrogen (NO_2) and oxygen (O_2) account for over 99 percent of the atmosphere and argon (Ar) almost 1

**Turbulence also may be of concern, but it is not addressed in this report.*

Figure A-10. Predicted tank signatures for central Europe under clear conditions.

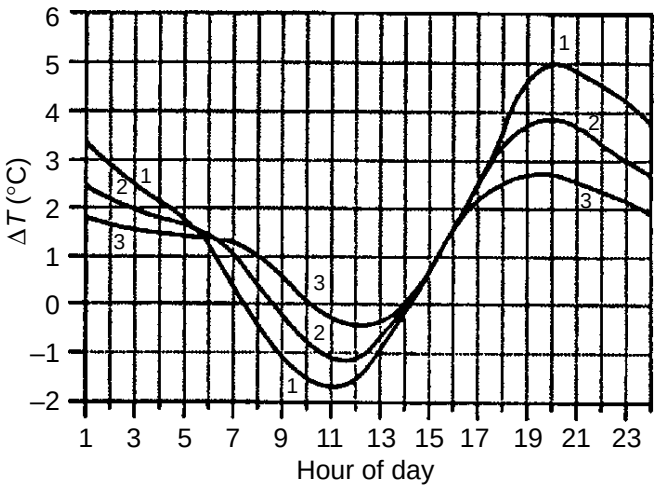

1. Summer
2. Spring/fall
3. Winter (referenced to 300 K background)

Figure A-11. Predicted tank signatures for central Europe under overcast conditions.

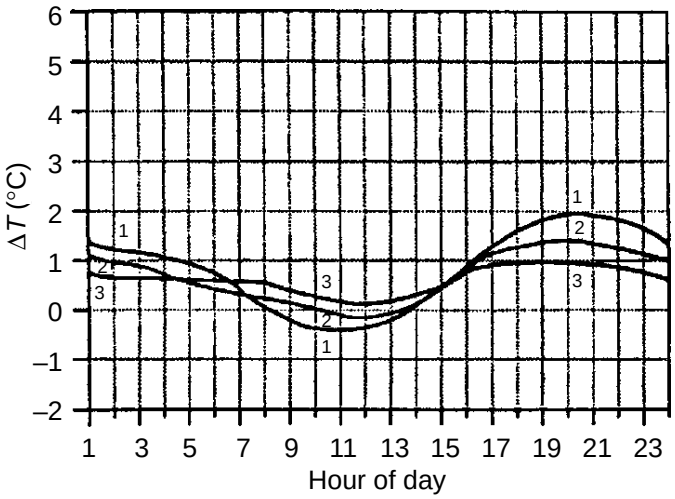

1 Summer
2 Spring/fall
3 Winter (referenced to 300 K background)

percent (see table A-2). Attenuation in the IR region is primarily due to water vapor and carbon dioxide (CO_2), and in the MMW region it is primarily due to water vapor and oxygen.

Figure A-12 shows the atmospheric attenuation in the MMW and IR regions [A-6]. The regions of local minimums are referred to as windows. The MMW windows are labeled in figure A-12. The 35- and 94-GHz windows are considered in this report. Note that the windows in the IR region are at 10 μm (8 to 12 μm) and 4 μm (3 to 5 μm).

Table A-2. Percentage of atmospheric constituents.

Constituent gas	Percentage of gas
N_2	78.04
O_2	20.95
Ar	0.93
CO_2	3×10^{-2}
H_2O	10^{-3} to 10^{-2}
Ne	1.8×10^{-3}
He	5.2×10^{-4}
NH_4	2×10^{-4}
Kr	1.14×10^{-4}
H_2	5×10^{-5}
N_2O	$\approx 5 \times 10^{-5}$
CO	$\approx 7 \times 10^{-6}$
O_3	0 to 7×10^{-6}
NO_2	0 to 2×10^{-6}
NO	0 to 2×10^{-6}

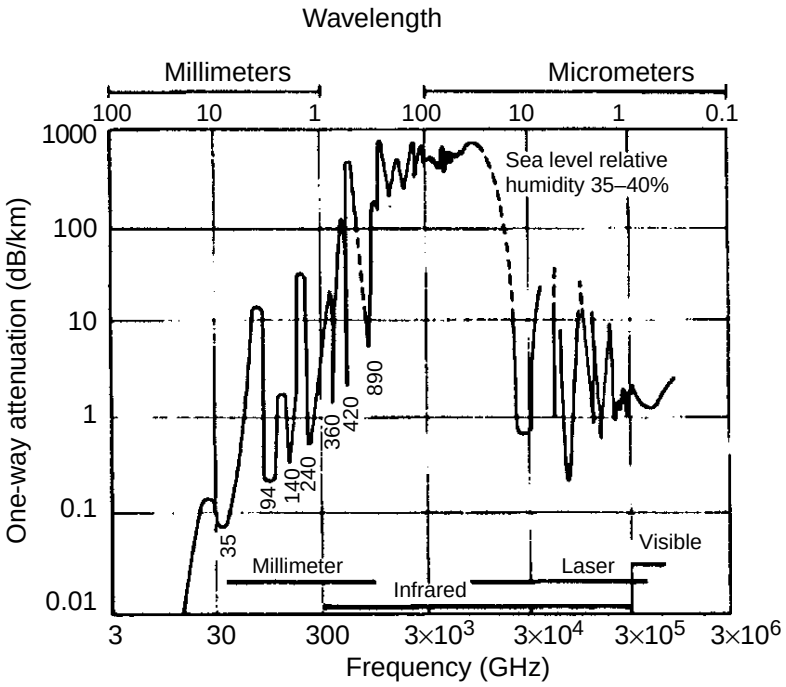

Figure A-12. Atmospheric attenuation for millimeter and infrared regions of spectrum.

Figures A-13 and A-14 more clearly show the MMW and IR bands, respectively. Note that figure A-14 shows atmospheric transmission rather than attenuation. The dip in the 3- to 5-μm band is due to carbon dioxide.

Particles from fog, which consists of suspended water droplets, rain, and haze, cause scattering of the incident radiation. Therefore, the signal in the desired direction is attenuated. Figure A-15 shows the effects of fog and rain on IR and MMW radiation [A-7].

Figure A-13. Atmospheric attenuation for millimeter region of spectrum.

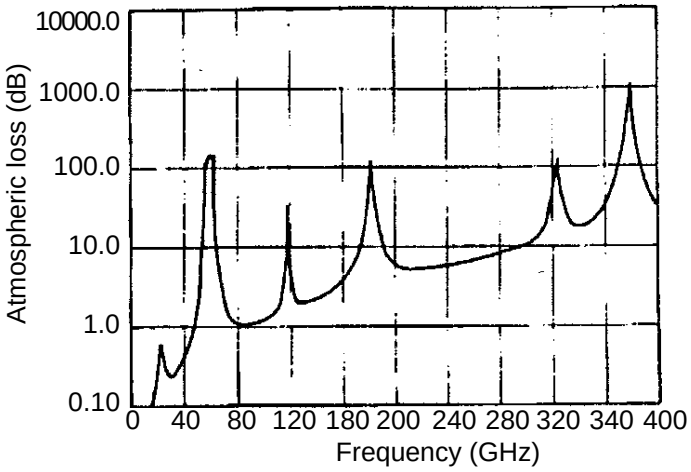

Figure A-14. Atmospheric attenuation for infrared region of spectrum.

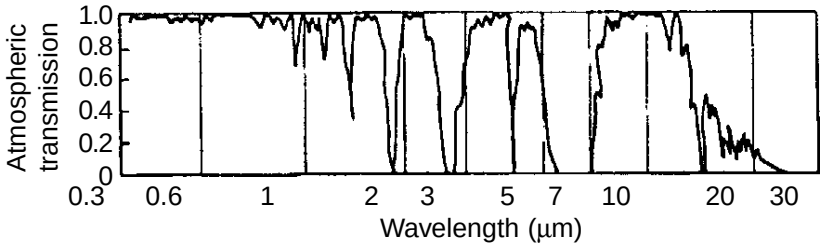

Figure A-15. Effects of fog and rain on IR and MMW radiation.

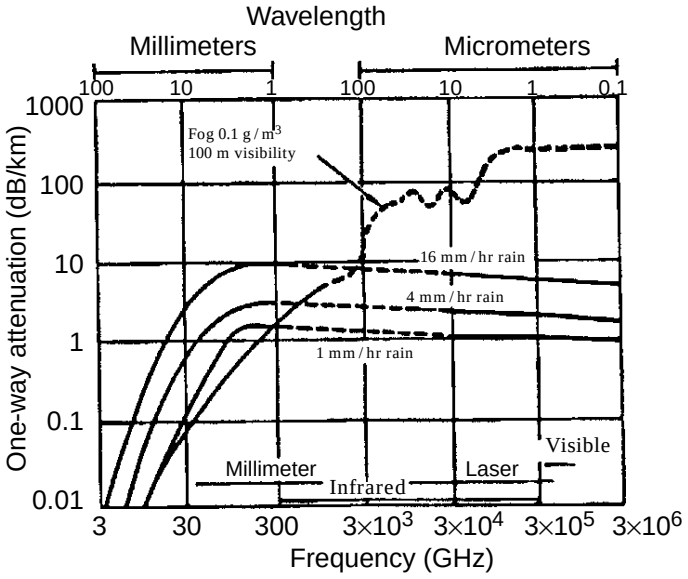

This figure shows minor differences in rain attenuation but major differences in fog attenuation on IR and MMW radiation.

The Battlefield Environment Directorate (BED) of ARL has an Electro-Optical Systems Atmospheric Library (EOSAEL) that contains several modules that give information about atmospheric effects. One of the modules is LOWTRAN, which is a relatively low resolution computer code that computes atmospheric transmittance in the IR region. Another module is near millimeter wave (NMMW), which computes atmospheric transmittance in the MMW region. In this report, LOWTRAN and NMMW were used to compute the atmospheric transmittance in the IR and MMW regions, respectively.

Appendix References

A-1. W. J. Wilson, R. J. Howard, A. C. Ibbott, G. S. Parks, and W. B. Ricketts, Millimeter-Wave Imaging Sensor, IEEE Trans. on Microwave Theory and Techniques. An equivalent notation is given by D. D. King, "Passive Detection," *Radar Handbook*, M. I. Skolnik, ed., McGraw-Hill, New York (1970).

A-2. P. Bhartia, and I. J. Bahl, *Millimeter Wave Engineering and Applications*, John Wiley and Sons, Inc., New York (1984).

A-3. James A. Ratches, *Static Performance Model for Thermal Imaging Systems*, Optical Engineering, **15**, 6 (November–December 1976).

A-4. J. Johnson, *Analysis of Image Forming Systems*, Proc. of Image Intensifier Symposium (October 1958).

A-5. *Infrared Imaging System Analysis*, DCS Corporation, Alexandria, VA (1988), reprinted by the Environmental Research Institute of Michigan, Ann Arbor, MI (1993).

A-6. S. A., Hovanessian, *Introduction to Sensor Systems*, Artech House, Norwood, MA, p 7 (1988).

A-7. S. A. Hovanessian, *Radar System Design and Analysis*, Artech House, Dedham, MA, p 297 (1984).

Distribution

Admnstr
Defns Techl Info Ctr
Attn DTIC-OCP
8725 John J Kingman Rd Ste 0944
FT Belvoir VA 22060-6218

Ofc of the Dir Rsrch and Engrg
Attn R Menz
Pentagon Rm 3E1089
Washington DC 20301-3080

Ofc of the Secy of Defns
Attn ODDRE (R&AT) G Singley
Attn ODDRE (R&AT) S Gontarek
The Pentagon
Washington DC 20301-3080

OSD
Attn OUSD(A&T)/ODDDR&E(R) J Lupo
Washington DC 20301-7100

Under Secy of Defns for Rsrch & Engrg
Attn Rsrch & Advncd Techlgy
Depart of Defns
Washington DC 20301

CECOM
Attn PM GPS COL S Young
FT Monmouth NJ 07703

CECOM NVESD
Attn AMSEL-RD-NV-ASD M Kelley
Attn AMSEL-RD-NV-TISD F Petito
Attn Techl Lib
FT Belvoir VA 22060

CECOM RDEC Elect System Div Dir
Attn J Niemela
FT Monmouth NJ 07703

CECOM Sp & Terrestrial Commctn Div
Attn AMSEL-RD-ST-MC-M H Soicher
FT Monmouth NJ 07703-5203

Dir of Assessment and Eval
Attn SARD-ZD H K Fallin Jr
103 Army Pentagon Rm 2E673
Washington DC 20301-0163

Dpty Assist Secy for Rsrch & Techl
Attn SARD-TT F Milton Rm 3E479
The Pentagon
Washington DC 20301-0103

Hdqtrs Dept of the Army
Attn DAMO-FDT D Schmidt
400 Army Pentagon Rm 3C514
Washington DC 20301-0460

MICOM RDEC
Attn AMSMI-RD W C McCorkle
Redstone Arsenal AL 35898-5240

Nav Rsrch Lab
Attn 4555 W Waters
Attn 7223 G Poe
Attn 7223 S Highley
4555 Overlook Ave SW
Washington DC 20375

Nav Weapons Ctr
Attn 472310 D S Rogala
China Lake CA 93555

Night Vision & Elec Sensors Dir
Attn AMSEL-RD-NV-OD J Ratches
10221 Burbeck Rd Ste 430
FT Belvoir VA 22060-5806

US Army Armament RDE Ctr
Attn SMCAR-FSP-A1 M Rosenbluth
Attn SMCAR-FSP-A1 R Collett
Picatinny Arsenal NJ 07806-5000

US Army Avn Rsrch, Dev, & Engrg Ctr
Attn T L House
4300 Goodfellow Blvd
St Louis MO 63120-1798

US Army CECOM NVESD
Attn AMSEL-RD-NV-RSPO A Tarbell
Mailstop 1112
FT Monmouth NJ 07703-5000

US Army CECOM Rsrch, Dev, & Engrg
Attn R F Giordano
FT Monmouth NJ 07703-5201

US Army Edgewood Rsrch, Dev, & Engrg Ctr
Attn SCBRD-TD J Vervier
Aberdeen Proving Ground MD 21010-5423

US Army Info Sys Engrg Cmnd
Attn ASQB-OTD F Jenia
FT Huachuca AZ 85613-5300

Distribution (cont'd)

US Army Materiel Cmnd
Attn AMCDM Dir for Plans & Analysis
5001 Eisenhower Ave
Alexandria VA 22333-0001

US Army Materiel Sys Analysis Agency
Attn AMXSY-D J McCarthy
Aberdeen Proving Ground MD 21005-5071

US Army Matl Cmnd
Dpty CG for RDE Hdqtrs
Attn AMCRD BG Beauchamp
5001 Eisenhower Ave
Alexandria VA 22333-0001

US Army Matl Cmnd
Prin Dpty for Acquisition Hdqrts
Attn AMCDCG-A D Adams
5001 Eisehnower Ave
Alexandria VA 22333-0001

US Army Matl Cmnd
Prin Dpty for Techlgy Hdqrts
Attn AMCDCG-T M Fisette
5001 Eisenhower Ave
Alexandria VA 22333-0001

US Army Missile Lab
Attn AMSMI-RD Advanced Sensors Dir
Attn AMSMI-RD Sys Simulation & Dev Dir
Attn AMSMI-RD-AS-MM G Emmons
Attn AMSMI-RD-AS-MM M Christian
Attn AMSMI-RD-AS-MM M Mullins
Attn AMSMI-RD-AS-RPR Redstone Sci Info Ctr
Attn AMSMI-RD-AS-RPT Techl Info Div
Redstone Arsenal AL 35809

US Army Natick Rsrch, Dev, & Engrg Ctr
Acting Techl Dir
Attn SSCNC-T P Brandler
Natick MA 01760-5002

US Army Rsrch Ofc
Attn G Iafrate
4300 S Miami Blvd
Research Triangle Park NC 27709

US Army Rsrch Ofc
Attn C Church
Attn B D Guenther
PO Box 12211
Research Triangle Park NC 27709-2211

US Army Simulation, Train, & Instrmntn Cmnd
Attn J Stahl
12350 Research Parkway
Orlando FL 32826-3726

US Army Tank-Automtv & Armaments Cmnd
Attn AMSTA-AR-TD C Spinelli
Bldg 1
Picatinny Arsenal NJ 07806-5000

US Army Tank-Automtv Cmnd Rsrch, Dev, & Engrg Ctr
Attn AMSTA-TA J Chapin
Warren MI 48397-5000

US Army Test & Eval Cmnd
Attn R G Pollard III
Aberdeen Proving Ground MD 21005-5055

US Army Test & Eval Cmnd
Attn STEWS-TE-AF F Moreno
Attn STEWS-TE-LG S Dickerson
White Sands Missile Range NM 88002

US Army Train & Doctrine Cmnd
Battle Lab Integration & Techl Dirctrt
Attn ATCD-B J A Klevecz
FT Monroe VA 23651-5850

US Military Academy
Dept of Mathematical Sci
Attn MAJ D Engen
West Point NY 10996

USA CRREL
Attn G D Ashton
72 Lyme Rd
Hanover NH 03755

USAASA
Attn MOAS-AI W Parron
9325 Gunston Rd Ste N319
FT Belvoir VA 22060-5582

USATEC
Attn J N Rinker
Attn P Johnson
7701 Telegraph Rd
Alexandria VA 22315-3864

Distribution (cont'd)

Nav Rsrch Lab
Attn 2600 Techl Info Div
4555 Overlook Ave SW
Washington DC 20375

Nav Surface Warfare Ctr
Attn Code B07 J Pennella
17320 Dahlgren Rd Bldg 1470 Rm 1101
Dahlgren VA 22448-5100

Nav Surface Weapons Ctr
Attn DX-21 Library Div
Dahlgren VA 22448

Nav Weapons Ctr
Attn 38 Rsrch Dept
Attn 381 Physics Div
China Lake CA 93555

GPS Joint Prog Ofc Dir
Attn COL J Clay
2435 Vela Way Ste 1613
Los Angeles AFB CA 90245-5500

Special Assist to the Wing Cmndr
Attn 50SW/CCX Capt P H Bernstein
300 O'Malley Ave Ste 20
Falcon AFB CO 80912-3020

USAFWright Lab
Attn WL/MMGS B Sundstrum
Attn WL/MMGS R Smith
101 W. Eglin Blvd Ste 287A
Eglin AFB FL 32542-6810

Sandia Natl Lab
PO Box 5800
Albuquerque NM 87185

DARPA
Attn B Kaspar
Attn ETO L Sobolewski
Attn ISO T Lawrence
Attn L Stotts
Attn TTO M McHenry
3701 N Fairfax Dr
Arlington VA 22203-1714

NASA Goddard Space Flight Ctr
Attn D M Le Vine
Attn J Wang
Attn P Racette
Greenbelt MD 20771

NASA Langley Rsrch Ctr
Attn B Kendall
Mail Stop 490
Hampton VA 23681-0001

ARL Electromag Group
Attn Campus Mail Code F0250 A Tucker
University of Texas
Austin TX 78712

Georgia Institite of Technology
Georgia Tech Rsrch Inst
Attn Radar & Instrmntn Lab R McMillan
Attn Radar & Instrmntn Lab T L Lane
Atlanta GA 30332

Univ of Massachusetts at Amherst
College of Engineering
Attn C Swift
Amherst MA 01003

Aerojet
Attn YU C Ngan
1100 W Hollyvale Stret Bldg 1
Azusa CA 91702

Dir for MANPRINT
Ofc of the Deputy Chief of Staff for Prsnnl
Attn J Hiller
The Pentagon Rm 2C733
Washington DC 20301-0300

Eviron Rsrch Inst of MI
Attn IRIA Lib
PO Box 134001
Ann Arbor MI 48113-4001

Gleason Research Associates
Attn T Gleason
5537 Twin Knolls Rd Ste 439
Columbia MD 21045-3272

Lockheed Martin Corp Elect & Missile Div
Attn E Weatherwax
5600 Sand Lake Rd Mail Stop 450
Orlando FL 32819

Millitech Corp
Attn R Huegenin
S Deerfield Rsrch Park PO Box 109
S Deerfield MA 01373

Distribution (cont'd)

Thermo Trex Corp
Attn J Galliano
Attn J Lovberg
10455 Pacific Center Court
San Diego CA 92121

TRW Space & Technology Div
Attn M Shoucri
Attn P Moffa
One Space Park
Redondo Beach CA 90278

US Army Rsrch Lab
Attn AMSRL-P-S-E B Perlman
FT Monmouth NJ 07703-5601

US Army Rsrch Lab
Attn AMSRL-WT-WB R A McGee
Aberdeen Proving Ground MD 21005

US Army Rsrch Lab
Attn AMSRL-CI-LL Techl Lib (3 copies)
Attn AMSRL-CS-AL-TA Mail & Records Mgmt

US Army Rsrch Lab (cont'd)
Attn AMSRL-CS-AL-TP Techl Pub (3 copies)
Attn AMSRL-SE J M Miller
Attn AMSRL-SE-E D Wilmot
Attn AMSRL-SE H Pollehn
Attn AMSRL-SE-E J Pellegrino
Attn AMSRL-SE-EE Z G Sztankay
Attn AMSRL-SE-EM B Riely (3 copies)
Attn AMSRL-SE-RM B Wallace
Attn AMSRL-SE-RM D Wikner
Attn AMSRL-SE-RM E Burke
Attn AMSRL-SE-RM H Dropkin
Attn AMSRL-SE-RM J Nemarich
Attn AMSRL-SE-RM J Silverstein
Attn AMSRL-SE-RM R Dahlstrom
Attn AMSRL-SE-RM R Wellman
Attn AMSRL-SE-RM G Simonis
Attn AMSRL-SE-RU J Sichina
Attn AMSRL-SE-SI T Kipp
Attn AMSRL-SE-SR D Rodkey
Adelphi MD 20783-1197

REPORT DOCUMENTATION PAGE

Form Approved
OMB No. 0704-0188

1. AGENCY USE ONLY *(Leave blank)*	2. REPORT DATE	3. REPORT TYPE AND DATES COVERED
	December 1997	Final, January to December 1995

4. TITLE AND SUBTITLE
Comparison of Infrared and Millimeter-Wave Imager Performance in Adverse Weather Conditions

5. FUNDING NUMBERS
PE: 62120A

6. AUTHOR(S)
Brian Riely

7. PERFORMING ORGANIZATION NAME(S) AND ADDRESS(ES)
U.S. Army Research Laboratory
Attn: AMSRL-SE (riely@arl.mil)
2800 Powder Mill Road
Adelphi, MD 20783-1197

8. PERFORMING ORGANIZATION REPORT NUMBER
ARL-TR-1301

9. SPONSORING/MONITORING AGENCY NAME(S) AND ADDRESS(ES)
U.S. Army Research Laboratory
2800 Powder Mill Road
Adelphi, MD 20783-1197

10. SPONSORING/MONITORING AGENCY REPORT NUMBER

11. SUPPLEMENTARY NOTES
AMS code: 622120.H1611
ARL PR: 6NE46F

12a. DISTRIBUTION/AVAILABILITY STATEMENT
Approved for public release; distribution unlimited.

12b. DISTRIBUTION CODE

13. ABSTRACT *(Maximum 200 words)*

This report compares the performance of infrared and millimeter-wave imagers in various weather conditions (rain, fog, clouds, and, to a lesser extent, snow). It then examines how often these weather conditions occur each season at selected areas around the world. The data for the frequency of occurrence of the adverse conditions were taken from a 1992 climatology module that used inputs from 795 meteorological stations around the world.

14. SUBJECT TERMS
Infrared imaging, millimeter-wave imaging

15. NUMBER OF PAGES
66

16. PRICE CODE

17. SECURITY CLASSIFICATION OF REPORT	18. SECURITY CLASSIFICATION OF THIS PAGE	19. SECURITY CLASSIFICATION OF ABSTRACT	20. LIMITATION OF ABSTRACT
Unclassified	Unclassified	Unclassified	UL

DEPARTMENT OF THE ARMY
U.S. Army Research Laboratory
2800 Powder Mill Road
Adelphi, MD 20783-1197